INVESTIGATION OF PHOTOCONDUCTIVITY

IN

CADMIUM SULFIDE

A Thesis

Presented to The

School of Graduate Studies

Addis Ababa

In Partial Fulfillment of the

Requirements for the Degree

Master of Science in Physics

by

Letemeskel Asfaw

June, 1984

ACKNOWLEDGEMENT

I would like to express my sincere gratitude to Dr. G. Kluge, my advisor, for the help and guidance from the beginning upto the end in writing this thesis. Without his efforts, it would have been impossible to get such experimental results.

I am very grateful to Dr. H.G. Neumann for providing the X-ray diffraction pattern of some of the layers.

I am also grateful to Dr. G. Ohms and Dr. D. Ohms for their valuable advice in the preparation of the layers, and to Dr. G. Busch for his advice in designing a measuring amplifier.

I would like also to acknowledge my indebtedness to Ato Girma Dagne for doing the technical work.

Financial support of the Addis Ababa University is gratefully acknowledged.

LIST OF FIGURES

LIST OF TABLES

ABSTRACT

In this thesis the photoconductivity of polycrystalline cadmium sulfide was investigated theoretically and experimentally. The theory shows that both a change in carrier conentration and mobility can contribute to the variation in conductivity under illumination depending on the doping level, trap concentration and light intensity. Thin-film polycrystalline layers of CdS were prepared by the chemical bath deposition technique. Doping with lithium was possible. X-ray investigation of the layers indicated that the layers are made up of very small crystallites. Annealing enhanced recrystallization increasing the crystallite dimension.

Besides polycrystalline CdS, monocrystalline and pressed CdS were used for photoconductivity measurements. The annealed layers showed a spectral photoresponse similar to the monocrystalline CdS with an absorption edge at 2.4eV. In order to measure the lifetime of the charge carriers, the photoconductive decay process was used. The lifetime was found to have a spectral dependence.

C O N T E N T S

INTRODUCTION

Photoconductivity, also called photoresistive effect or internal photoeffect, is the variation of the electrical resistance of a semiconductor or an insulator due to illumination by light.

It was Willoughby Smith [1,p.1] in 1873 who noticed for the first time a photoresistive effect in illuminating selenium and since then hundreds of photoconducting materials have been found. In parallel, theoretical explanations of the basic mechanisms of the photoconductive process in semiconductors and insulators have been suggested and also experimentally checked. The investigations of photoconductivity have played an important role in the determination of important properties of semiconductors and thus have contributed a great deal to the recent wide-spread application of semiconducting materials. For instance, the forbidden energy gaps of a number of semiconductors and the ionization energies of impurity atoms have been determined by means of the spectral response of photoconductivity in the infrared region though now such measurements can also be done by determination of the optical absorption [2,p.452]. On the other hand, refined investigations of the photoconductive process have been made possible by the development of high purity semiconductor technology especially by providing crystals of defined purity and known doping.

After a wide investigation of monocrystalline semiconductors the research has become more concerned with polycrystalline

and amorphous materials, too. Polycrystalline layers offer the advantage of low costs with preparation methods fairly adaptable to large scale production techniques. One such thin-film polycrystalline representative is cadmium sulfide which is the subject of this thesis.

Application of photoconductors are in vidicon television cameras, photoresistors, light detectors (also infrared), light sensitive switches, electrophotography, etc. Polycrystalline thin-film cadmium sulfide is furthermore one of the most promising solar cell materials (window material) [3]. Together with suitable absorbers like Cu_2S or CdTe [3,4] cheap photovoltaic cells can be formed which are an interesting alternative to monocrystalline and polycrystalline silicon solar cells. Therefore, the preparation of polycrystalline cadmium sulfide and the investigation of its electrical and photoelectrical properties constitute a direct contribution to the development of thin film cadmium-sulfide-based solar cells.

After a review of the photoconductivity theory of monocrystalline semiconductors in chapter 1, models for the photoconductivity of polycrystalline layers are discussed in chapter 2. Chapter 3 describes the preparation of thin-film polycrystalline cadmium sulfide by the chemical bath deposition method and in chapter 4 the electrical and photoelectrical measurements are presented and discussed.

CHAPTER 1

PHOTOCONDUCTIVITY IN MONOCRYSTALLINE SEMICONDUCTORS

1.1 Semiconductors

A semiconductor is a solid whose band gap energy E_g is less than about 3eV. For a semiconductor without any impurities (intrinsic semiconductor) the Fermi level E_F lies approximately at the middle of the band gap and the conductivity increases strongly with increasing temperature. The increase is due to an increase in the free carrier concentrations, ie. of electrons n and holes p, as given by [5, p.198]

$$n = N_C \exp\left(-\frac{E_C - E_F}{kT}\right) = N_C \exp\left(-\frac{E_g}{2kT}\right) \qquad (1)$$

and

$$p = N_V \exp\left(-\frac{E_F - E_V}{kT}\right) = N_V \exp\left(-\frac{E_g}{2kT}\right) \qquad (2)$$

where N_C and N_V are the effective density of states in the conduction and valence band, respectively, and E_C and E_V are the band edge energies of these two bands, k is the Boltzmann constant and T the absolute temperature.

For an extrinsic semiconductor, unlike the intrinsic one, states exist in the forbidden band as a result of imperfections which can be due to impurity atoms (dopants), or due to crystal defects, vacancies, etc. If the ionization energies of such states in the forbidden bandgap (donor or acceptor levels) is so low that already

low temperatures are sufficient for their ionization, high free carrier concentrations are observed (high electron concentration in an n-type semiconductor and high hole concentration in a p-type semiconductor). In accordance, the Fermi level is shifted upwards towards the conduction band for an n-type or downwards towards the valence band for a p-type semiconductor. If n_i is the electron and hole concentration of the intrinsic sample, the following relation holds also for the extrinsic case:

$$n \cdot p = n_i^2 ,$$

ie. the higher the electron or hole concentration, the lower the hole or electron concentration, respectively. Cadmium sulfide can only be prepared as high-conductivity n-type material [4; 9, p.452] . Anion-(S)-vacancies behave as donors as do group III (eg. indium) and group VII impurities, cation-(Cd)-vacancies act as acceptors together with group I and V impurities (compensation). The only means by which a p-type condition is claimed to have been induced is by ion bombardment with bismuth [9, p.449]. CdS has a direct bandgap with a bandgap energy of E_g= 2.582 eV at T=0K and E_g= 2.42 eV at 300K [8, p.210] . The bonds of CdS are of ionic and covalent character with an ionic content of 69% [8, p.85] .

1.2 Electrical Conductivity

The conductivity of a substance is determined by the concentration and the so-called mobility of free charge carriers.

In the absence of an external electric field, the charge carriers diffuse in a random motion with a net charge flow of zero. But, when there is an external electric field (E) applied to the two ends of the semiconductor, the charge carriers drift with a preferred direction besides their diffusion. The drift velocities of electrons and holes are given by

$$\begin{aligned} v_n &= - \mu_n E \\ v_p &= \mu_p E \end{aligned} \tag{3}$$

where μ_n and μ_p are the electron and the hole mobilities respectively, ie. their average drift velocity per unit electric field. The total current is the sum of electron and hole current and the current density becomes

$$\vec{j} = \vec{j}_n + \vec{j}_p = - en\vec{v}_n + ep\vec{v}_p \tag{4}$$

or with eq.(3)

$$\vec{j} = e(n\ \mu_n + p\ \mu_p)\ \vec{E}. \tag{5}$$

e stands for the elementary charge.

The electrical conductivity σ is defined as

$$\vec{j} = \sigma\vec{E}$$

so that the conductivity of the semiconductor becomes

$$\sigma = e(n\ \mu_n + p\ \mu_p) \tag{6}$$

1.3 Photoconductivity.

Photoconductivity involves the absorption of energy from an electromagnetic radiation which excites (creates) additional free charge carriers in a semiconductor or an insulator. Possible excitations that contribute directly to an increase in free carrier concentration are shown on Fig. 1 [1.p.43].

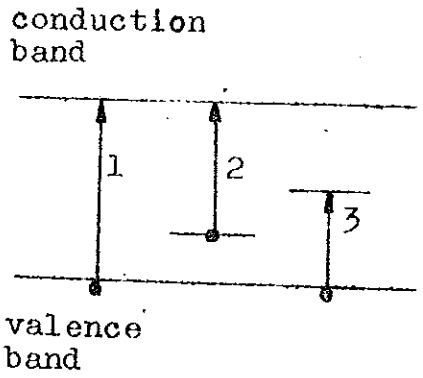

Fig. 1: Absorption and excitation.

Absorption of a photon with an energy larger than E_g excites an electron from the valence band into the conduction band (thus creating a free electron-hole pair). In this generation process, the related change in free electron concentration (Δn) equals the change in free hole concentration (Δp). Processes 2 and 3 show the ionization of an impurity level leading to additional free electrons (Δn) and the excitation of an electron from the valence band in

to an impurity level thus increasing the hole concentration (Δp). Another absorption mechanism that indirectly contributes to an increase of free electron and hole concentration is exciton absorption [8.p.432].

In accordance with eq.(6) the photoconductivity, which is by definition the change in conductivity due to illumination, becomes:

$$\sigma_{pc} = \Delta\sigma = e\{\Delta(n\mu_n) + \Delta(p\mu_p)\}$$

$$= e\{\mu_n\Delta n + n\Delta\mu_n + \mu_p\Delta p + p\Delta\mu_p\} \quad (7)$$

In a crystal the change in conductivity is attributed to the change in carrier concentration Δn, Δp and not to a variation of the mobilities $\Delta\mu_n$, $\Delta\mu_p$ [5], and from eq. (7) the photoconductivity becomes

$$\sigma_{pc}(\lambda) = \Delta\sigma(\lambda) = \{\mu_n\Delta n(\lambda) + \mu_p\Delta p(\lambda)\}e \quad (8)$$

The photoconductivity is strongly wavelength (λ) dependent because the spectral response has to reflect the optical properties of the semiconductor. For most of the photoconuctors the mobilities μ_n and μ_p or the changes of the carrier concentrations Δn and Δp are much different so that in eq. (8) one term is dominating and the other can be omitted. Backus [9] reports for CdS $\mu_n = 340\ cm^2/Vs$ and $\mu_p = 615\ cm^2/Vs$ and lifetimes (cf. part 1.4) to be $\tau_n = 100s$ and $\tau_p = 10^{-2}s$. As shown in section 1.4, (eq.(18)) the

saturation values of Δn and Δp therefore will be different by a factor 10^4 and hence the photoconductivity is mainly attributed to an electron current:

$$\sigma_{pc} \cong e \mu_n \Delta n.$$

Negative photoconductivity, ie. a decrease in conductance with respect to that of thermal equilibrium in the dark has been observed in thin-single crystals of CdS when subjected to infrared radiation (infrared quenching of photoconductivity). The infrared radiation excites holes from discrete states inside the energy gap into higher excited levels close to or inside the valence band. These holes recombine via recombination centres with free electrons leading to negative photoconductivity [2].

1.4 Generation, Recombination, Trapping, Lifetime.

If a semiconductor is illumunated, free electrons and/or holes are generated at a generation rate g. If there no means existed to return the charge carriers to their initial state the conductivity would have to increase continuously. In reality this is not the case because the carriers have a limited lifetime τ, ie. a limited time to contribute to the conductivity, for they are either trapped in a trapping centre during which they cannot contribute to the conductivity; or recombine in a recombination centre thus electron-hole pairs being annihilated. Recombination and trapping centres appear in states that exist in the forbid-

den band region which are attributed to foreign impurities, structural defects, etc. in the crystal. Recombination occurs when this type of centre captures a free electron and holds it until emptied by capturing a hole, while trapping is just only capturing either a hole or an electron and releasing it after some time [6].

There are different forms that recombination may take according to the way how the energy is released in the process of recombination of the electron-hole pairs [1.p.301]:

a) radiative recombination-in this type of recombination a photon is radiated

b) non-radiative recombination-where a phonon is released in the process of electron-hole recombination

c) Auger recombination-the energy released during recombination is given to other particles which gain a high velocity called "hot" particles which in the process of collision give their energy to the lattice which appears as a phonon.

d) exciton recombination-The energy of recombining particles appears in a bound electron-hole pair.

The lifetime mentioned above is the 'free lifetime' (the time a carrier is free to contribute to the conductivity) in difference to the 'excited lifetime' which is the total time the carrier is between its excitation and recombination, including the time it is trapped.

The surface ofacrystal is a macroscopic deviation from the crystal periodicity and for this reason the effects of trapping and recombination are different at these boundaries, compared with those of the bulk material. Therefore, the effective lifetime of a free carrier includes two components, a bulk lifetime τ_b and a surface lifetime τ_s , which are related by [6.p.330]:

$$\frac{1}{\tau_{eff}} = \frac{1}{\tau_b} + \frac{1}{\tau_s} \qquad (9)$$

The lifetime of charge carriers is connected to the photoconductivity gain G of a photoconductor which is the number of free charge carriers that pass between the electrodes per number of created electron-hole pairs per second. If t* denotes the so-called transit time of a carrier which is the time that a carrier needs to pass through a semiconductor of length ℓ (interelectrode spacing) at a drift velocity v, the photoconductivity gain becomes the ratio between the lifetime τ and the transit time t* . Considering both types of carriers (n,p) Bube [1.p.60] gets for $\tau <$ t*

$$G = \frac{\tau_n}{t_n^*} + \frac{\tau_p}{t_p^*} \qquad (10)$$

The transit time is derived from the drift velocity eq. (3) as

$$t^* = \frac{\ell^2}{\mu V}$$

where V stands for the voltage applied between the electrodes. Hence, the photoconductivity gain can be rewritten as

$$G = (\mu_n \tau_n + \mu_p \tau_p) \frac{V}{\ell^2} \qquad (11)$$

The maximum performance of a photoconductor is attained for $\tau > t^*$, and gains greater than unity can be obtained [4,8,p.430].

A free carrier diffuses an average distance (L) before it recombines (diffusion length) [5] which is given by

$$L = \sqrt{D\tau} \quad \text{(diffusion length)} \tag{12}$$

where D is the diffusion constant:

$$D = \mu\frac{kT}{e} \quad \text{(Einstein relation)}. \tag{13}$$

Eqs. (12) and (13) provide a functional connection between lifetime and mobility:

$$\mu_n\tau_n = \frac{eL_n^2}{kT} \; ; \; \mu_p\tau_p = \frac{eL_p^2}{kT} \; . \tag{14}$$

If n_o is the free electron concentration in the dark and n(t) the concentration under illumination at time t, the lifetime τ_n can be used to define a recombination rate r_n by

$$r_n = \frac{n(t)-n_o}{\tau_n} \tag{15}$$

assuming that the lifetime is independent of n(an equivalent recombination rate can be formulated for holes). Considering the time dependence of the free electron concentration n(t), the continuity equation becomes

$$\frac{d(\,n(t)-n_o)}{dt} = \frac{d\,n(t)}{dt} = g_n - r_n = g_n - \frac{n(t)-n_o}{\tau_n}; \tag{16}$$

the generation rate g_n being opposed by the recombination rate r_n. If the light (generation) is switched on at t = 0

integration gives for $\Delta n(t) = n(t) - n_o$

$$q\,\Delta n(t) = g\tau_n\{1 - \exp(-\frac{t}{\tau_n})\}, \qquad (17)$$

For $t > 0$ the carrier concentration increases exponentially and approaches for $t >> \tau$ the saturation value

$$\Delta n_{sat} = g\tau_n \qquad (18)$$

If after reaching the saturation value Δn_{sat} the light is switched off (at $t' = 0$), then

$$\Delta n(t') = g\tau_n \exp(-\frac{t'}{\tau_n}) \qquad (19)$$

for $t' > 0$; the photoconductivity ceases exponentially. Eq. (19) represents the basic equation for the photoconductive decay method for the measurement of the lifetime of charge carriers. τ_n is the effective 'excited lifetime'. The photoconductive decay therefore reveals trap parameters, too.

CHAPTER 2

PHOTOCONDUCTIVITY OF POLYCRYSTALLINE SEMICONDUCTORS.

2.1 General Aspects of Polycrystalline Semiconductors.

Polycrystalline materials are made up of small crystallites packed together in a certain order with a transitional region between them. They are usually found as thin layers formed on a substrate. Unlike single crystal semiconductors, their electric and photoelectric properties will be affected due to the transitional region.

Bulk photoconductors (semiconductors) respond to radiation in much the same way as do thin films and the thickness of the device does not affect its inherent property. However, most photoconductors generally exhibit strong absorption over a limited portion of the spectrum and so utilize only a very thin layer of the order of microns of the material. Thus, easier preparation methods of thin-film layers that can be attained economically make polycrystalline materials alternatives that replace single crystals for special applications.

2.2 Review of Existing Theories.

Theories of conductivity and photoconductivity of polycrystalline CdS were developed in line with those for other polycrystalline semiconductors such as lead salts [10, 11] which are of great potential as infrared detectors due to

their narrow band gap and polycrystalline silicon (polysilicon), which is of importance for low cost solar cells and electronic units [12].

Throughout the investigation of photoconductivity in polycrystalline materials a certain controversy has been sustained: Is the photoconductivity due primarily to an increase in carrier density (Δn , Δp) or due to the increase in mobility ($\Delta\mu_n$, $\Delta\mu_p$) of the free carriers? The answer to this question is less an experimental difficulty than a problem of theoretical interpretation of conductivity and mobility measurements. In contrast to single crystal semiconductors the carrier density and mobility are spatially inhomogeneous within the polycrystalline material. Observable quantities of the photoconductive thin film, on the other hand, are a result of the average properties of the polycrystalline material. This brings about the necessity to have models available that provide the relationship between the observable (macroscopic) quantities and microscopic properties of the inhomogeneous sample.

Common to all the different models is a consideration of the polycrystalline materials as to be composed of small crystallites which are joined together by a transitional region. Volger [13] and Petritz [10] considered the transitional region as being composed of a different material than the crystallites, eg. of oxides.

Volger [13] treated the resulting polycrystalline structure as a resistance network (geometric model) whereas Petritz [10] assigned to this intergranular layer a potential barrier. In addition he argued that a great number of trapping centres for minority carriers occur at the grain boundary so that this model can be called as "grain boundary trapping model". He interpreted the photocurrent as a majority current caused by electron-hole pair generation (primary process) due to light absorption within the crystallites. A secondary mechanism is trapping of minority carriers at the intergranular trapping centres which are extracted from the crystallites. Due to this trapping the barrier height is modulated and as a consequence the mobility increases. Petritz showed that the mobility is thermally activated for the current flow is limited by thermionic emission of carriers

$$\mu^* = \mu_o \exp\left(-\frac{eV_B}{KT}\right) \qquad (20)$$

where eV_B is the potential barrier height. The origin of the potential barrier is not discussed in further detail.

In extending the grain boundary trapping model, Seto [12] proposed a mechanism that clarifies the origin of the potential barrier. He considered the intergranular layer that provides the transition between adjacent crystallites, being of the same composition as the crystallites, but of strongly disordered structure. Due to this high number of

imperfections, a great number of grain-boundary states are brought about which represent trapping centres for the free carriers. Hence, free carriers are trapped by these traps at the grain boundary leaving behind a depleted region. This space charge region causes a nonuniform electric potential and consequently a band bending and a potential barrier.

Seto's discussion was aimed on the investigation of the (dark) conductivity of polysilicon.

Orton etal. [14] used Seto's model as a basis for the discussion of photoconductivity and combined it with the former proposal of Petritz: Light absorption leads to a generation of electronhole pairs. The created electrons (for n-type material) increase the free carrier concentration whereas the holes become trapped at the grain boundary (secondary process). As a result, the grain boundary cannot support a fully depleted grain as before so that it shrinks. H.C Card [15] discusses that under optical illumination the potential barrier which he describes as the diffusion potential decreases from its dark value. Then, the mobility, as can be seen from eq. (20), increases. Thus, the grain boundary trapping model explains both the increase in carrier concentration and the mobility under illumination of polycrystalline materials.

Quantitative Analysis of the Grain-Boundary-Trapping Model

Although thin-film polycrystalline CdS is a three dimensional structure, a one-dimensional analysis exhibits the characteristic features of the material.

Following Seto [12] the one-dimensional grain boundary trapping model considers the polycrystalline film to be composed of idential crystallites having a grain size of L_g cm

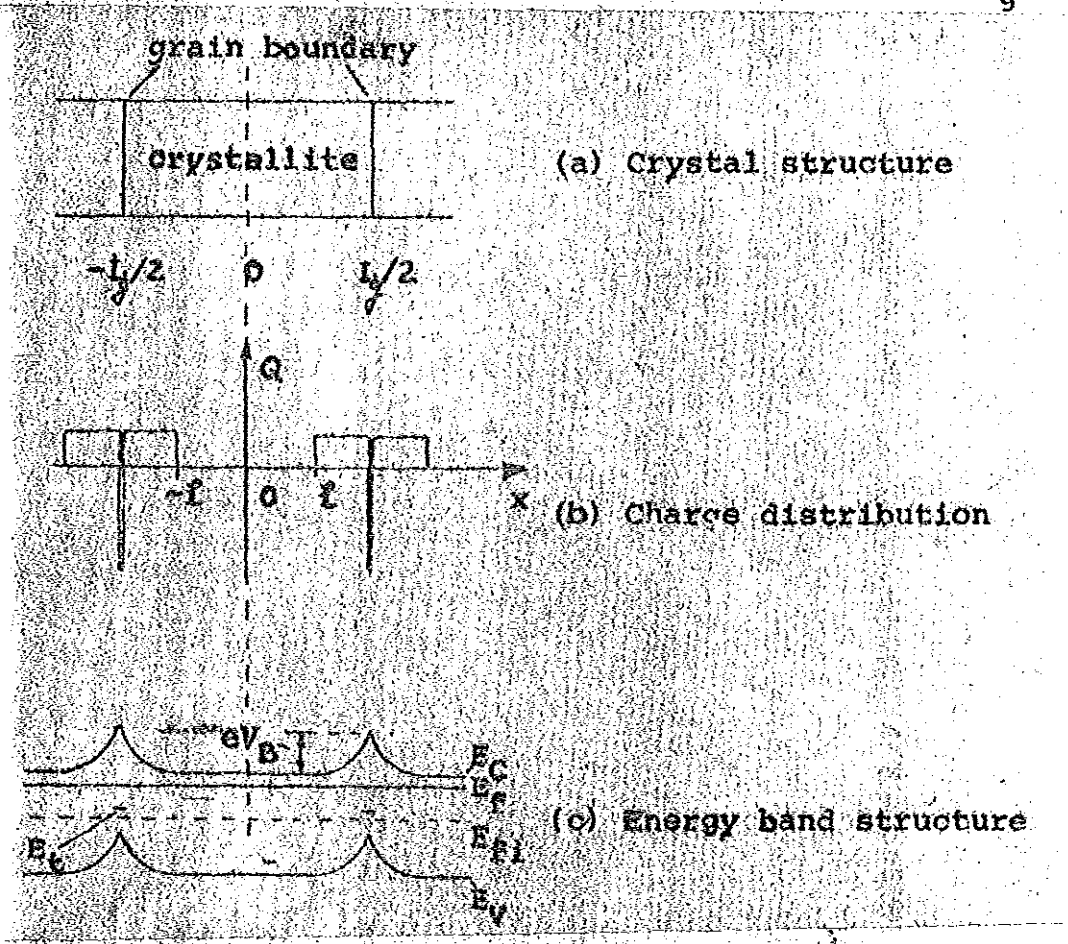

Fig. 2: a) Model of crystal structure
b) Charge distribution
c) Energy band structure
of a n-type polycrystalline semiconductor [12].

The crystallites contain uniformly distributed impurity atoms of concentration N_d/cm^2 which should be totally ionized. The grain boundary is of negligible thickness with a trap concentration of Q_t/cm^2 at a single energy level E_t. The traps are initially neutral and become charged by trapping majority carriers (electrons). As a result of the electron trapping, the crystallites are partly or completely depleted (Fig. 2 (b)) from electrons depending on the relation between the number of trapping states Q_t occupied and the free electron concentration $N_d L_g$. For $Q_t > N_d L_g$ the traps are not all occupied and the crystallites are completely depleted whereas for $Q_t < N_d L_g$ all traps are occupied and the crystallites are depleted only partially. The depleted regions constitute a space charge region (of ionized donors) in which the related electric potential can be calculated by integrating Poisson's equation:

$$\frac{d^2V}{dx^2} = \frac{eN_d}{\epsilon} \qquad \text{for} \quad \ell < |x| < \frac{L_g}{2} \tag{21}$$

where ℓ is the width of the depleted region as shown on Fig. 2 (b), and ϵ the dielectric permitivity. An abrupt, depletion approximation is assumed to be valid and mobile carriers in the depleted region are neglected in writing Poisson's equation. The voltage is

$$V(x) = V_C^o + \frac{eN_d}{2\epsilon}(x - \ell)^2 \tag{22}$$

with boundary conditions $\frac{dV}{dx}|_{x=\ell}=0$ and $V(x)|_{x=0}=V_C^0$ (V_C^0 denotes the potential of the conduction band edge at the centre of the crystallite). The parabolic potential causes the energy bands to bend upwards by $eV(x)$ (Fig. 2.(c)).

For $Q_t > N_d L_g$ the crystallites are completely depleted (ie. $\ell=0$) and the potential reduces to

$$V(x) = V_C^0 + \frac{eN_d}{2} x^2 \quad |x| < \frac{L_g}{2} \quad , \tag{23}$$

the potential barrier height takes the value

$$V_B = V(\frac{L_g}{2}) - V(0) = \frac{eN_d}{8\varepsilon} L_g^2 \tag{24}$$

which increases linearly with N_d keeping the other parameters constant.

It is possible to evaluate the mobile carrier conentration using Boltzmann's statistics:

$$n(x) = N_C \exp\{-\frac{eV(x) - E_F}{kT}\} \quad , \tag{25}$$

N_C being the effective density of states in the conduction band. Hence, mobile carriers also occur in the depleted region which were neglected following Seto's lead for the calculation of the potential. The electron concentration {Eq. (25)} is position dependent and the question arises, which value to insert into the expression for the conductivity

$$\sigma = en\mu \, .$$

The spatially averaged value

$$n_a = \frac{1}{L_g} \int_{-L_g/2}^{L_g/2} n(x)\,dx \qquad (26)$$

appears to be most appropriate [12, 14] and the conductivity gets the form

$$\sigma = e\, n_a \mu$$

Also μ is spatially in homogeneous. To retain the commonly used relationship $\sigma = en\mu$, a so called effective mobility is to be taken

$$\mu_{eff} = \frac{\sigma}{e\, n_a} \,. \qquad (27)$$

n_a can be calculated by inserting eqs. (23) and (25) into eq. (26) :

$$n_a = \frac{1}{eL_g} \exp\{-\frac{eV_C^0 - E_F}{kT}\} \left(\frac{2\varepsilon kT}{N_d}\right)^{\frac{1}{2}} \operatorname{erf}\{\left(\frac{e^2 N_d}{2kT}\right)^{\frac{1}{2}} \frac{L_g}{2}\} \,. \qquad (28)$$

For $Q_t < N_d\, L_g$, the crystallites are only partly depleted so that $\ell > 0$ and an analogeous calculations give a barrier height of

$$V_B = \frac{eQ_t^2}{8\varepsilon N_d} \,. \qquad (29)$$

The potential barrier versus doping concentration N_d is plotted schematically in Fig. 3. It increases linerly with N_d for $Q_t > N_d\, L_g$, attains a maximum at $N_d\, L_g = Q_t$ and decreases rapidly as $\frac{1}{N_d}$ for $Q_t < N_d\, L_g$.

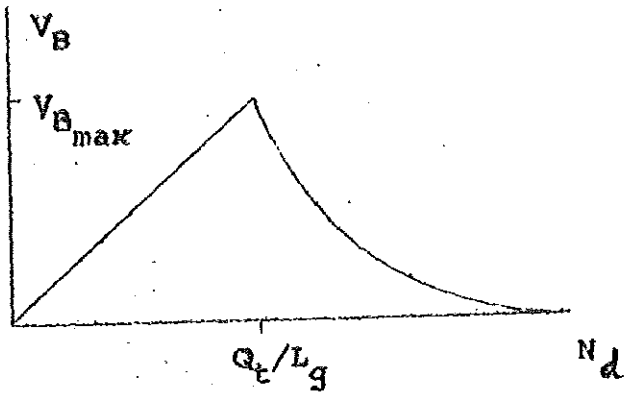

Fig. 3: Scheme of the variation of the barrier height versus the doping concentration N_d

If within the undepleted region the carrier concentration is assumed to be that of single crystalline CdS, the average carrier concentration becomes

$$n_a = n_b \left| (1 - \frac{Q_t}{N_d L_g}) + \frac{1}{eL_g} \left(\frac{2\pi kT\varepsilon}{N_d}\right)^{\frac{1}{2}} \mathrm{erf}\left\{\frac{eQ_t}{2}\left(\frac{1}{2\varepsilon kTN_d}\right)^{\frac{1}{2}}\right\} \right| . \quad (31)$$

Seto [12] has demonstrated that the resistance of the polycrystalline material is caused mainly by the grain boundary and not by the bulk of the crystallite and secondly, after applying a voltage across the specimen, the current is a result of thermionic emission, where the tunneling current can be neglected due to the relatively large width of the barrier. If the applied voltage drops by V_a across a grain, the thermionic emission current density, j_{th}, across the grain boundary is

$$j_{th} = e\, n_a \left(\frac{1}{2\pi m^* kT}\right)^{\frac{1}{2}} \exp\left(-\frac{eV_B}{kT}\right) V_a . \quad (32)$$

where m* is the effective mass and it is assumed that $eV_a << kT$. Since the conductivity is related to the current, ie.

$$j_{lR} = \sigma E = \sigma \frac{V_a}{L_g} ,$$

the mobility using eqs. (32) and (27) can be written as

$$\mu_{eff} = eL_g \left(\frac{1}{2\pi m^* kT}\right)^{\frac{1}{2}} \exp\left(-\frac{eV_B}{kT}\right) \qquad (33)$$

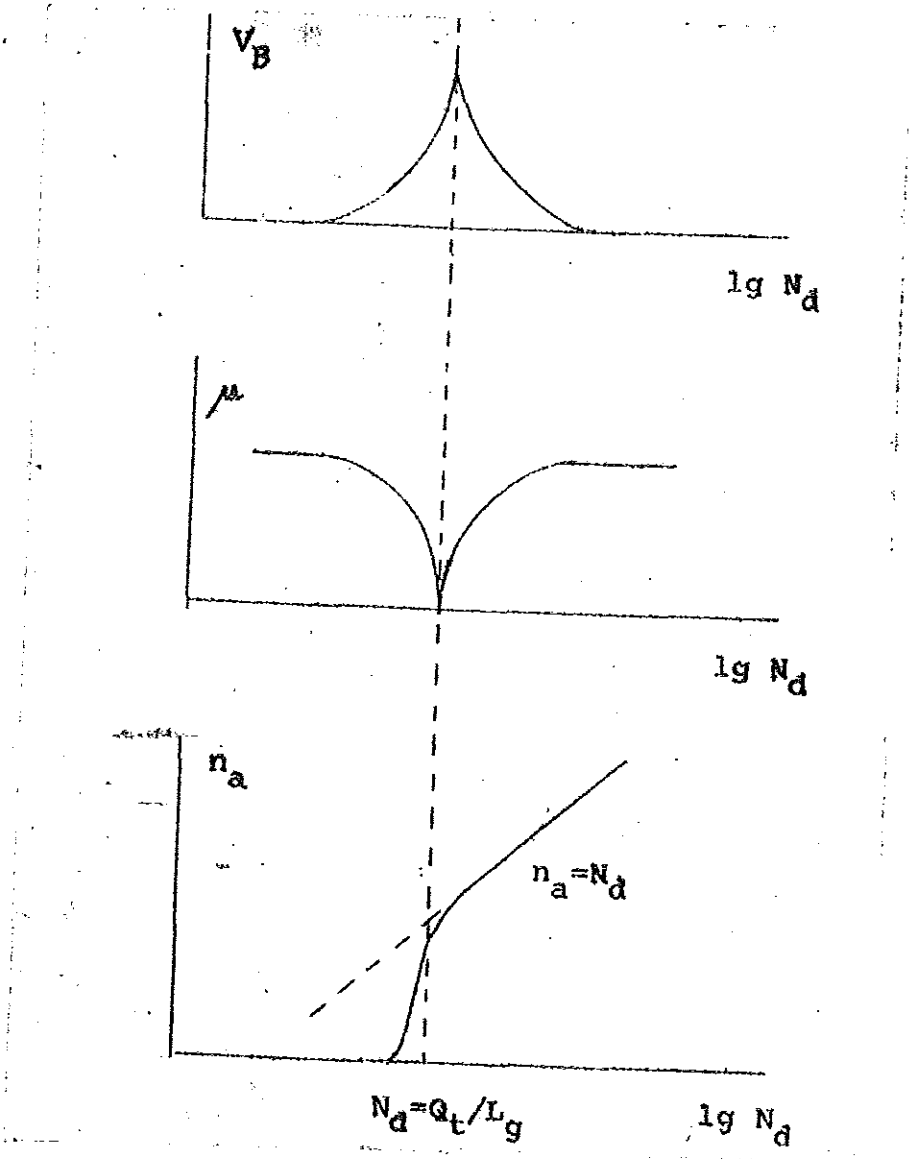

Fig. 4: Behavior of barrier height, mobility and average carrier density versus doping concentration [14].

The results are summarized in Fig. 4 . The barrier height eV_B approaches a maximum at $L_g N_d = Q_t$ while according to eq. (33) the mobility reaches its minimum at this point. For large and small N_d the mobility approaches that of a single-crystalline CdS. The average carrier concentration n_a increases abruptly as $L_g N_d$ approaches Q_t and for a further increase in doping concentration it takes the value of N_d.

The Fermi level E_F is determined by equating the number of carriers trapped to the total number of trapping states.

$$L^* N_d = \frac{Q_t}{2 \exp\left(\frac{E_t - E_F}{kT}\right) + 1} \tag{34}$$

where $L^* = L_g$ for $Q_t > L_g N_d$ and $L^* = L_g - 2\ell$ for $Q_t < N_d L_g$.

Thus, $$E_F = E_t - kT \ln \tfrac{1}{2}\left(\frac{Q_t}{N_d L_g} - 1\right) . \tag{35}$$

A scheme of these two cases is given in Fig. 5.

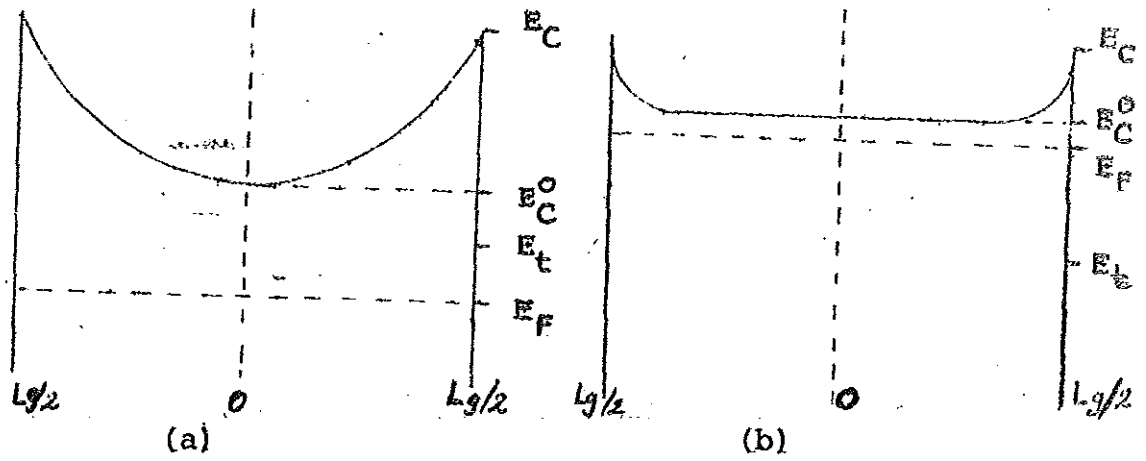

Fig. 5: Band Bending Profile

a) $Q_t > N_d L_g$ (b) $Q_t < N_d L_g$.

For $Q_t > L_g N_d$, the Fermi level is well below E_c^o and the number of free carriers is small indicating that states at E_t are rarely occupied. For $Q_t < L_g N_d$ states at E_t are nearly all occupied and the number of carriers is high because the Fermi level is close to the conduction band (which is similar to that of single crystals of the same doping).

Under illumination the quasi-Fermi level for electrons moves upwards while the Fermi level which determines the trap occupancy moves down. Hence, the density of free electrons in the conduction band increases independent whether Q_t is larger or smaller than $N_d L_g$.

On the other hand, the hole occupancy of the trap level increases as the quasi-Fermi level, which determines the hole occupancy, moves downwards. For $Q_t > N_d L_g$ and low light intensities, the whole crystallite remains depleted and the potential barrier is found from eq. (24). Consequently, the effective mobility does not change. If the light intensity is increased for the case $Q_t > N_d L_g$, the hole occupancy of the trap levels can increase so strongly that the barrier cannot support a completely depleted grain. As a result a flat portion of the band within the crystallite occurs, the barrier height decreases leading to an increase of the mobility. Thus, the electron concentration and mobility change, both contributing to the photoconductivity.

For $Q_t < N_d L_g$ the depletion width will shrink always under illumination, so that the carrier concentration and the mobility will always change under illumination.

The quantitative relationship between Δn_a and $\Delta \mu_{eff}$ could be derived on the assumption that all holes generated due to light absorption are trapped at the grain boundary. But it is to be expected that quantitative differences between theoretical and experimental results occur because important characteristics like grain size distribution as well as a non-uniform trap-level E_t are not considered.

For the work presented, such calculation and refined measurements are not included because both mobility and carrier concentration as well as the doping level N_d and trap concentration Q_t are not available. Therefore, a quantitative comparison with experimental results is not possible. But the represented theories enlighten the qualitative relationship between measured quantities and microscopic paramenters in photoconductive processes of polycrystalline semiconductors.

2.4 Calculation of the Absorbance of Thin-Film Photoconductors Deposited on Glass Substrate.

Only the part of electromagnetic radiation that is absorbed by the semiconductor can contribute to photoconductivity. Therefore, the optical properties of the semiconductor,

especially the wavelength dependence of its absorption coefficient $\alpha(\lambda)$, is of great importance for the spectral response of photoconductivity.

A thin-film photoconductor, without considering the electrical contacts, consists of an absorbing layer of the semiconductor of thickness d, refractive index $\tilde{N} = N + iK$ (where N is the refractive index and K is the absorption index), deposited on a non-absorbing substrate (glass) of refractive index N_g (Fig. 6).

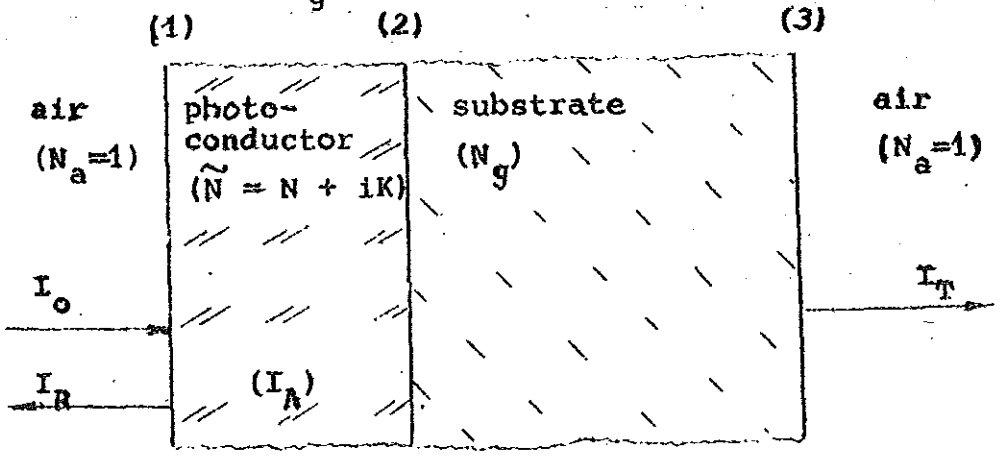

Fig. 6: Scheme of the photoconductor.

If monochromatic light of wavelength λ and intensity I_o is incident on a sample, a part $I_R(\lambda)$ will be reflected, a part $I_A(\lambda)$ absorbed and the remaining part $I_T(\lambda)$ leaves the semiconductor as transmitted light. Introducing the reflectance R, absorbance A and transmittance T by

$$R(\lambda) = \frac{I_R(\lambda)}{I_o}$$

$$A(\lambda) = \frac{I_A(\lambda)}{I_o} \qquad (36)$$

$$T(\lambda) = \frac{I_T(\lambda)}{I_o}$$

the law of conservation of energy demands the following relation

$$R(\lambda) + A(\lambda) + T(\lambda) = 1. \qquad (37)$$

The absorbance $A(\lambda)$ of the semiconductor is the determining term for the photoconductive response. For completely coherent and monochromatic light, for which the light amplitudes are to be added, R, A and T are given by Born and Wolf [16].

Petrowa et al. [17] have obtained the relevant expressions for R, A and T for the case that the coherence length of the light is larger than the film thickness d but smaller than the substrate thickness D. On the other hand, for the case that the films are not of an exactly constant thickness and the incident radiation is not perfectly monochromatic or that the coherence length is very small, as it is true in real situations, interference effects cancel each other or do not occur. Thus, R, A and T will be equal to those values obtained by an addition of light intensities

as for incoherent light. In what follows is discussed the exact expressions for R, A and T for the system of Fig. 6 for incoherent light incidence.

When light is incident on the air/semiconductor/glass/air system shown on Fig. 6, the reflected, absorbed and transmitted intensities are a result of multiple reflections. An expression for the absorbance A of an absorbing medium with refractive index $\tilde{N}$, thickness d, deposited on glass substrate of refractive index N_g can be calculated. To start with at first the glass substrate is assumed to be of infinite thickness and thus not causing reflection (Fig. 7).

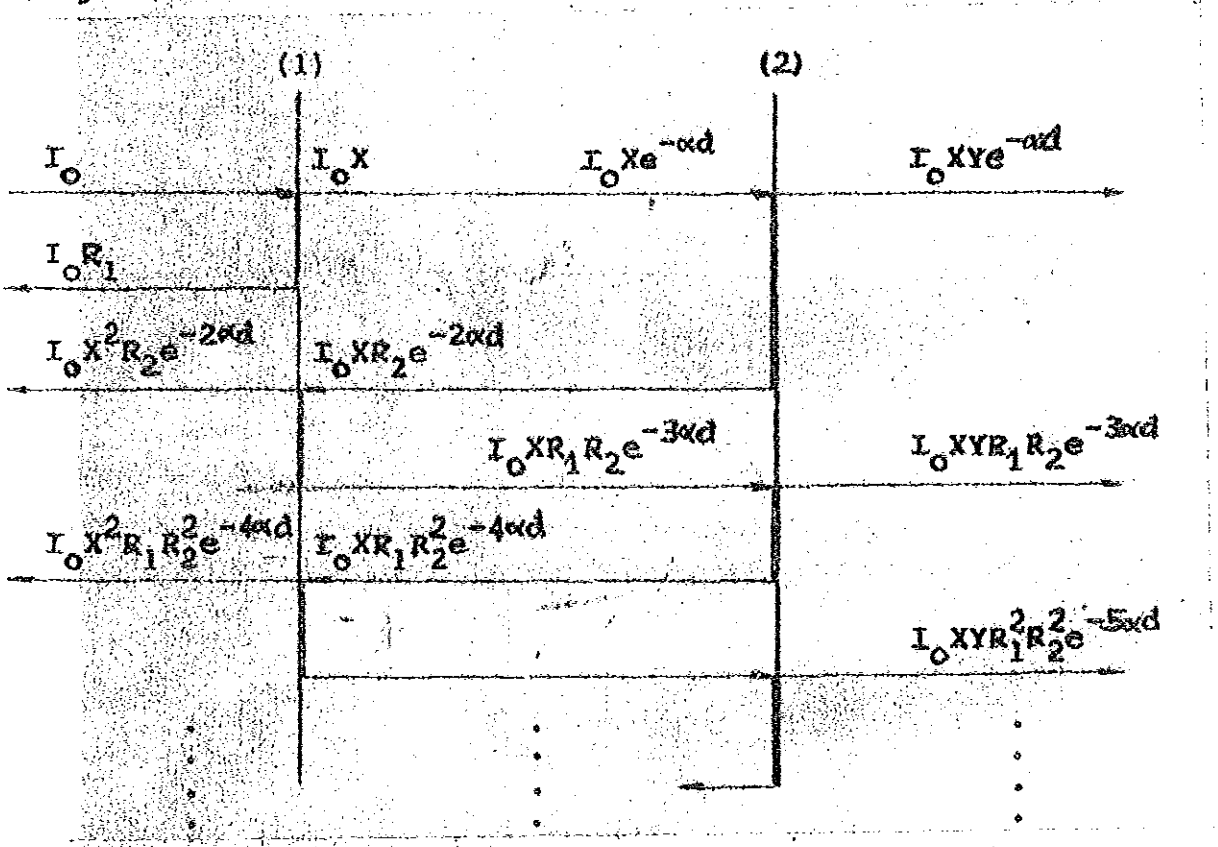

Fig. 7: Multiple reflections of air/semiconductor/ glass system (where $X = 1-R_1$ and $Y = 1-R_2$)

The reflectance, absorbance and transmittance of this subsystem are found by summing up all the multiple reflections:

$$R^{(12)} = R_1 + \frac{(1-R_1)^2 R_2 \exp(-2\alpha d)}{1-R_1 R_2 \exp(-2\alpha d)} , \tag{38}$$

$$A^{(12)} = \frac{(1-R_1)\{1+R_2 \exp(-\alpha d)\}\{1-\exp(-\alpha d)\}}{1-R_1 R_2 \exp(-2\alpha d)} , \tag{39}$$

$$T^{(12)} = \frac{(1-R_1)(1-R_2)\exp(-\alpha d)}{1-R_1 R_2 \exp(-2\alpha d)} , \tag{40}$$

where the sequence of superscripts indicate the direction of incident light and R_1 and R_2 are given by

$$R_1 = \frac{(N-1)^2 + K^2}{(N+1)^2 + K^2} , \tag{41a}$$

$$R_2 = \frac{(N-N_g)^2 + K^2}{(N+N_g)^2 + K^2} . \tag{41b}$$

For further calculations the equivalent values for light incident from the opposite direction are needed, which are found by interchanging R_1 and R_2 :

$$R^{(21)} = \frac{(1-R_2)^2 R_1 \exp(-2\alpha d)}{1-R_1 R_2 \exp(-2\alpha d)} + R_2 , \tag{42}$$

$$A^{(21)} = \frac{(1-R_2)\{1+R_1 \exp(-\alpha d)\}\{1-\exp(-\alpha d)\}}{1-R_1R_2 \exp(-2\alpha d)}, \qquad (43)$$

$$T^{(21)} = \frac{(1-R_2)(1-R_1)\exp(-\alpha d)}{1-R_1R_2 \exp(-2\alpha d)}. \qquad (44)$$

Because $T^{(12)} = T^{(21)}$ both will be abbreviated by $T^{()}$.

So far, we have considered the glass substrate to extend to infinity where in real situations it is interrupted by air of refractive index N_a. Including reflections from interface 3, a situation as in Fig. 8 arises.

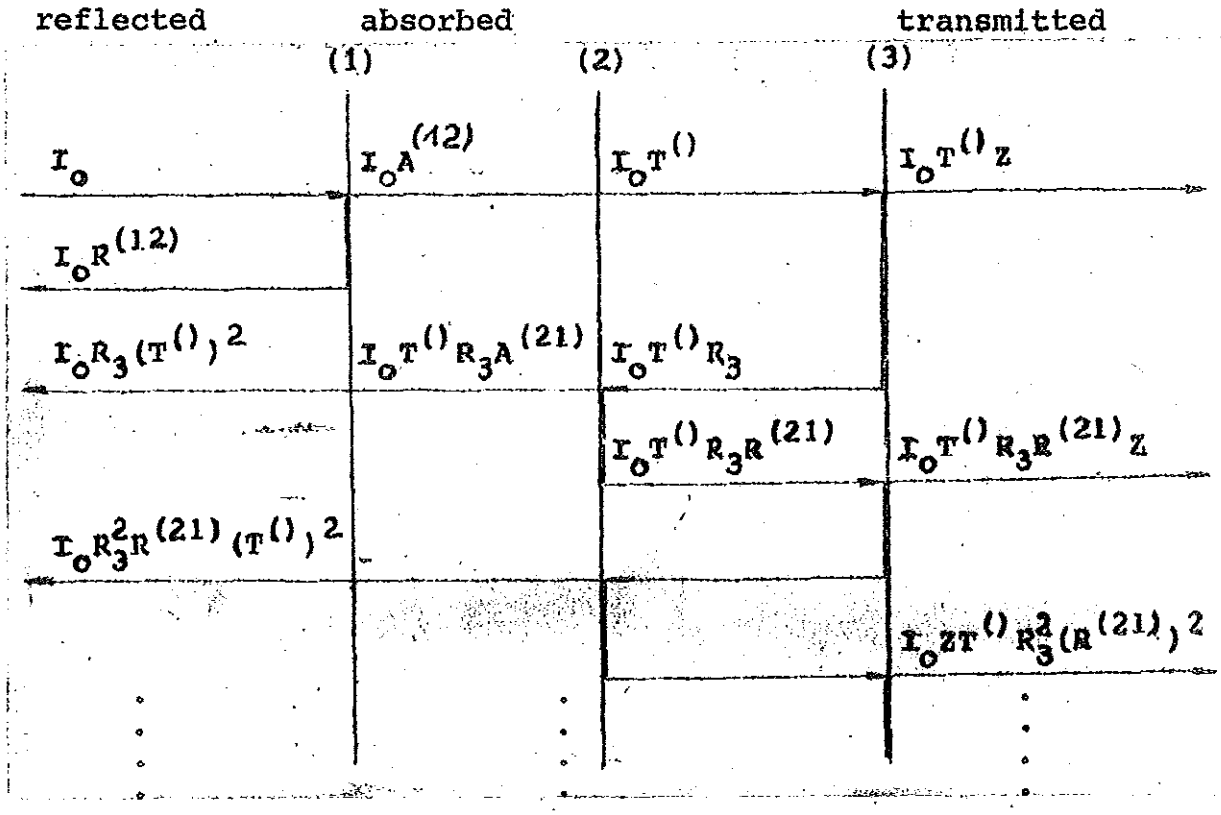

Fig. 8: Multiple reflections of air/semiconductor/glass/air system ($z = 1-R_3$).

The total absorbance is the sum of all the absorbed portions;

$$A = A^{(123)} = A^{(12)} + \frac{T^{(\ )}\ R_3\ A^{(21)}}{1-R_3\ R^{(21)}} \qquad (45)$$

where

$$R_3 = \frac{(N_g - 1)^2}{(N_g + 1)^2} \qquad (46)$$

Since $R_3 \cong 0.05$ and $R^{(2,1)} < 1$, approximation can be made by neglecting $R_3.R^{(21)}$ in the denominator without causing any significant error which is equivalent to dropping the contributions of light reflected more than once at the interface 3. The second term can as well be dropped for it contains R_3 multiplied by terms that are smaller than one which is equivalent to the assumption that the interface (3) reduces only the transmitted light by a factor $(1-R_3)$ without causing any reflections. Lastly, the denominator of eq. (39) can be approximated by 1, so that the total absorbance can be approximated by

$$A = (1-R_1)(1+R_2\ e^{-\alpha d})(1-e^{-\alpha d}). \qquad (47)$$

2.5 Relation Between Absorbance and Generation Rate.

The generation of charge by a photoconductor is proportional to the number of absorbed photons per unit time. If the intensity of the incident radiation is I_o (energy per unit area and time), an amount of $A.I_o$ is absorbed

within the photoconductor of thickness d and area $\omega \cdot \ell$. The number of absorbed photons per unit time for a monochromatic source is

$$\frac{I_o A}{h\nu} \cdot \omega \cdot \ell$$

where ν is the frequency of light.

The generation rate (g) which is the increase in free charge carriers per time and volume is defined as

$$g = \frac{d(\Delta n)}{dt}$$

where

$$d(\Delta n) = d\frac{(\Delta N)}{V} = d\frac{(\Delta N)}{(\omega \ell d)} \qquad (48)$$

$d\frac{(\Delta N)}{dt}$ is proportional to the number of absorbed photons per unit time

$$d\frac{(\Delta N)}{dt} = \eta \frac{I_o A}{h\nu} \quad \omega \cdot \ell$$

where η is the quantum efficiency (ie. the probability that an absorbed photon will generate free charge carriers):

$$g = \frac{d(\Delta n)}{dt} = \frac{d\,(\Delta N)}{V \cdot dt}$$

$$= \eta \cdot \frac{I_o A \cdot \omega \ell}{h\nu \cdot \omega \ell d} = \eta \frac{I_o A}{h\nu d} \cdot \qquad (49)$$

A is given by eqs. (45) and (47).

For the above derivation it was assumed, as proposed by Petritz [10], that the change in carrier concentration due to illumination is spatially constant within the film of thickness d, although the absorption profile is non-uniform. This is the case if the diffusion length is larger than the film thickness, so that a non-uniform carrier concentration in the direction perpendicular to the film always becomes uniform by diffusion. Hence, it is without influence, in which depth a photon is absorbed and generates electron-hole pairs, so that the total absorbance A can be used for calculation.

H.C. Card [15] considers an arrangement for measurement as in Fig. 9 and assumes that a carrier diffusion in the x-direction does not take place for the grain boundaries occur in a vertical direction. The absorption of light is a function of the film thickness

$$dI = - \alpha I \, dx \tag{50}$$

which makes the number of absorbed photons spatially non-uniform.

According to eq. (47) it would be possible to calculate the absorption profile within the thin film. As a result, the photoconductivity will depend on the thickness . As shown on the figure, the measured current is the average current so that the x-dependece of the photocurrent cannot be recognized. Therefore, assuming

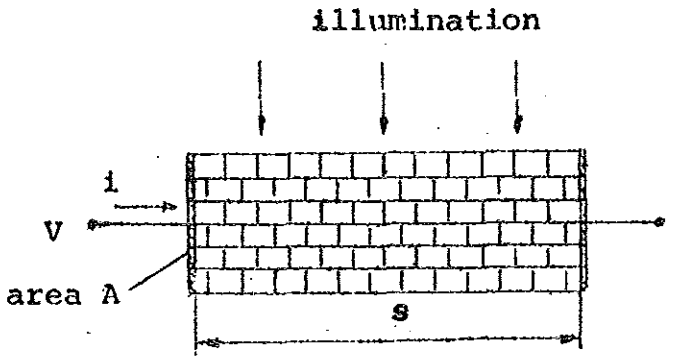

$$\sigma = \frac{si}{VA}$$

Fig. 9: Determination of conductivity.

a proportionality between charge carrier concentration (n) and photoconductive effect, a treatment as done before is justified. Furthermore, reflections at the interfaces support this discussion by making the absorption profile more smooth.

CHAPTER 3

PREPARATION OF POLYCRYSTALLINE CdS THIN-FILMS.

3.1 The Chemical Bath Deposition.

Different preparations methods exist in competition leading to comparable polycrystalline cadmium sulfide thin-films. Thermal evaporation and sputtering [3] have been widely used for the preparation of CdS thin-film and need an expensive set-up which are operated at high temperatures. On the other hand, spray pyrolysis [3, 18] , screen-printing and sintering [19] , and chemical bath deposition can be used to produce large area thin-film layers economically at relatively low temperature, The chemical bath depositon method has been known for sometime [20] , but the electrical and photoelectrical properties are less investigated. Because of the availability of the equipment needed for this method, it was chosen to apply this method for the preparation of CdS thin-films.

3.2 Preparation Technique.

CdS layers are prepared by mixing thiourea in an alkalline solution containing a cadmium salt, in this case cadmium acetate. The cadmium acetate reacts with the ammonia solution to form a complex tetrammonium compoound which dissociates the thiourea. The chemical reaction for the formation of CdS films is given by

$$Cd^{+2} + (NH_2)_2\,CS + 2OH^- \rightarrow CdS + NH_2\,CN + 2H_2O\,. \qquad (51)$$

There are two possibilities for CdS layer formation. One is the ion to ion combination from the colloidal solution directly on the substrate and second the deposition of CdS from the precipitate in the solution onto the substrate.

The deposition was made on a glass-substrate that was cleaned by immersing it in chromium acid. The glass-substrates were immersed in the reaction beaker and rotated at 120r.p.m in order to stir the aqueous solution of the reactants.

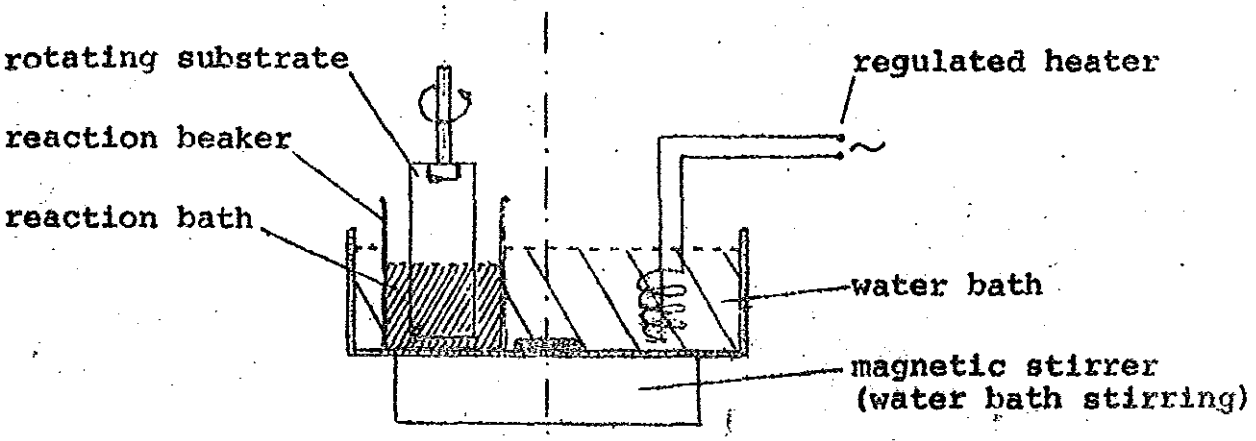

Fig. 10: Experimental set-up for the chemical bath deposition.

The films produced are influenced by the ambient, ie. rate of substrate rotation (stirring), temperature of deposition, rate of heating, pH-value, duration of deposition, and concentration of reactants in the solution. A series of

layers were prepared according to a programme for the variation of the parameters. The best filmswere obtained by mixing

1.25 ml	0.5 M	$Cd(CH_3COO)_2$,
10 ml	0.1 M	$(NH_2)_2CS$,
10 ml	14 M	NH_4OH ,
2.5 ml	dist.	H_2O .

All were mixed at room temperature and the mixture was heated at a rate of about 1.5°C/min up to 65°C with the substrate immersed in the reaction beaker and rotated 120 rpm to ensure vigorous stirring. Once the optimum deposition temperature has been reached, the deposition was continued for an additional 10 minutes while the temperature is kept constant. Finally, the layers were taken out and rinsed with distilled water and dried in air. The thickness of these films, was measured as described in part 3.3, and amounted to 5 µm.

The following variations of the parameters resulted in thick, porous, powdery and rough layers in contrast to the optimum results obtained which are adherent, reflecting and uniform (non-powdery):

- extension of the deposition time to 15 and 20 minutes after reaching the final temperature,
- increase of the final temperature to 75°C,

- increase in cadmium acetate concentration,
- decrease of the ammonia concentration and thus decrease of the pH-value of the reaction solution.

Films prepared by decreasing the cadmium acetate concentration maintaining the thiourea concentration constant are comparable to those ones obtained under optimum conditions except that the thickness of the layers was smaller. A decrease in the final temperature of deposition to 50°C strongly slowed down the deposition rate. This affects the thickness of the layers which could not be compensated by an extension of the deposition time to 90 minutes.

An intended doping of the films is possible [21]. Doping with lithium can be done by adding 1.5 ml 0.01 M LiF to the reaction mixture which gave layers similar to those without doping. A similar procedure was done to dope the layers with copper by adding 1.5 ml 0.01 M $CuSO_4$ which gave a negligible CdS deposition. The reason could be a formation of copper complexes which hinder the deposition.

Other variations tried were an immersion of the substrate after having attained the final temperature and a double bath deposition (repetition of the deposition on the same substrate using a fresh bath). The first resulted in thin layers, while the latter increased the thickness of the uniform layer to 13 µm. Hence, a repeated deposition allows the preparation of the films of desired thickness.

The deposition was done on a glass-substrate which was already coated with a highly conducting and transparent thin film of tin oxide (SnO_2), that can serve as the back contact for a CdS/Cu_2S solar cell. The result was similar to the deposition on a clean glass-substrate.

Table 1. Samples Prepared.

Sample number	Compound Concentration compared with O C	Deposition temp. (°C)	Deposition time (min)	Specialiites
1		70	15	
2	200% $Cd(CH_3COO)_2$	65	30	
3		55	30	
4a				
4b	O C	65	15	annealed at 120°C for 1 hr and 70 Pa
5	200% $Cd(CH_3COO)_2$	65	10	
6a			10	
6b	OC	65	40	annealed at 120°C for 1 hr at 70 Pa
7a	400 %		10	
7b	$Cd(CH_3COO)_2$	65	20	
8	75 %			
9	50 % of NH_4OH	65	10	
10	25 %			
11a				
16	OC + Li doped	65	10	
19				

Table 1 (cont.)

11b	OC + Li doped	65	20	
12 14 15	OC + Cu doped	65	10	
13	OC	65	10	
17 18 20	OC + Li doped	65	10	double bath deposition
23a	OC	65	10	thiourea added after reaching 65°C
23b	OC	65	10	substrate immersed after reaching 65°C
24a 24b	OC + Li doped	65	10	substrate immersed after reaching 65°C
25a 25b	60% $Cd(CH_3COO)_2$	65	10 15	
II*	OC	65	10	annealed at 120°C for 1 hr at 70 Pa, annealed at 550°C for 1 hr in air
III*	OC + Li doped	65	10	annealed at 300°C for 20 min at 0.013 Pa

3.3 Measurement of the Film Thickness

The electrical and photoelectrical measurements as described in chapter 4.provide the dark-and the photo-resistance. The related resistivities and conductivities can only be calculated if the geometrical dimensions of the sample, especially its thickness d, are known. Furthermore, the film thickness is needed for a determination of the optical constants of the films from transmission measurements, as well as for a quantitative evaluation of the film deposition by the method applied.

The thickness of the films was measured using a Spencer microscope. An ocular micrometer containing 100 equidistant intervals (ocular micrometer scale units = OMSU) was calibrated by comparison with a 2 mm long object micrometer of interval spacing 10 µm. For a 10-fold-ocular and objectives of 10-, 45-, and 100-fold magnification, one OMSU was found to correspond to

14.8 µm for 10x10,
3.3 µm for 10x45, and
1.45µm for 10x100 total magnification.

For the measurement of the film thickness, the films were positioned vertically and illuminated from below. Because of the strong absorption by the vertical films they appeared black when observed through the micorscope and the strong contrast between the films and the adjacent media (substrated, air) allowed the measurement of the thickness with a good accuracy.

3.4 Investigation of the Film Structure by X-ray Diffraction: Results.

When X-ray radiation is incident on a crystal it is scattered from its periodically spaced atoms. The diffracted rays interfere coherently and cause intensity maxima at certain angles Θ given by Bragg's relation

$$2\, d_{hkl} \sin \Theta = m\lambda \,, \tag{52}$$

where m is the diffraction order and d_{hkl} the interplaner spacing of planes with Miller indices (hkl).

The stable form of cadmium sulfide is hexagonal structure (wurtzite structure), which is the only one for which single crystals can be grown, with the following lattice constants [22]

$$a = (4.1367 \pm 0.0003)\ \text{Å}\,,$$

$$b = (6.7161 \pm 0.0005)\ \text{Å}\,.$$

Values measured by other authors [23] differ slightly. The dependence of the interplanar spacing d_{hkl} on the Miller indices hkl, and a and c for a hexagonal structure is given by [24]

$$d_{hkl}^{-2} = \frac{4}{3}\,\frac{h^2 + hk + k^2}{a^2} + \frac{l^2}{c^2}\,. \tag{53}$$

Table 2 presents d_{hkl}-values of hexagonal CdS observed by Swanson et al. [23] that can be used for indexing diffraction pattern if hexagonal CdS is expected.

Table 2: d_{hkl}-values of hexagonal CdS according to Swanson et al. [23]

hkl	d_{hkl} |Å|	Θ^* |grad|
100	3.583	18.64
002	3.357	19.94
101	3.160	21.24
102	2.450	27.86

*) for m = 1 and λ = 2.29 Å (chromium-K_α-radiation)

Cadmium sulfide films can be either hexagonal or cubic or both [8] . Cook et al. [22] report a lattice constant of a = 5.839 Å for cubic CdS (zinc blende-fcc structure). For a cubic structure d_{hkl} is given by

$$d_{hkl}^2 = \frac{a^2}{h^2 + k^2 + \ell^2} \qquad (54)$$

and Bragg reflections occur for the fcc-structure only if the hkl are unmixed (all odd or all even) [7,p.61]. Expected reflections for the lowest (hkl) are calculated in Table 3.

Table 3: d_{hkl}-values of expected diffraction maxima of cubic CdS (zinc blende structure) with a = 5.839Å

hkl	d_{hkl} |Å|	Θ^*) |grad|
111	3.371	19.86
200	2.920	23.09
220	2.064	33.69
311	1.761	40.57

*) for m = 1 and λ = 2.29 Å (Cr-K_α)

In the process of CdS preparation, especially during its annealing, CdS can be oxidized to form cadmium oxide which has a face-centered structure with a lattice constant $a = 4.695 \text{ Å}$ [11].

Possible diffraction maxima caused by CdO are given in Table 4 [25].

Table 4: Expected d_{hkl}-values of fcc CdO

hkl	d_{hkl} |Å|	Θ*) |grad|
111	2.711	24.99
200	2.348	29.19
220	1.660	43.61
311	1.416	53.98

*) for m = 1 and $\lambda = 2.29$ Å (Cr-K_α)

The X-ray diffraction spectra of the films prepared by the chemical bath deposition technique were recorded by Dr. Neumann (Physics Department of the Wilhelm-Pieck-University Rostock/GDR). The radiation used was Cr-K_α ($\lambda = 2.29$ Å). Six layers have been investigated which were prepared according to the optimum-condition procedure with and without doping and a post-annealing as listed in Table 5.

Table 5: Preparation conditions of the layers investigated by X-ray diffraction

layer	doping with Li	double bath deposition	annealing
I			no
II			at 120°C for 1 hr at 70 Pa
III	X		no
IV	X		at 120°C for 1 hr at 70 Pa
V	X	X	no
VI	X	X	at 120°C for 1 hr at 70 Pa
II*	layer II, in addition annealed at 550°C in air for 1 h		
III*	layer III, in addition annealed at 300°C for 20min at 0.013 Pa		

The spectra found are shown in Fig. 11 together with the spectra of CdS-powder. CdS powder shows clear peaks at 18.6°, 20.0° and 21.3° which relate to the interplanar spacing 3.58Å, 3.36Å and 3.16Å respectively in agreement with Bragg's relation

$$2d \sin \Theta = m\lambda$$

for $m = 1$.

From Fig. 11(a), the diffractions planes can be identified as (100), (002) and (101) planes of hexagonal CdS.

Fig.11: X-ray spectra of the layers listed in Table 5.

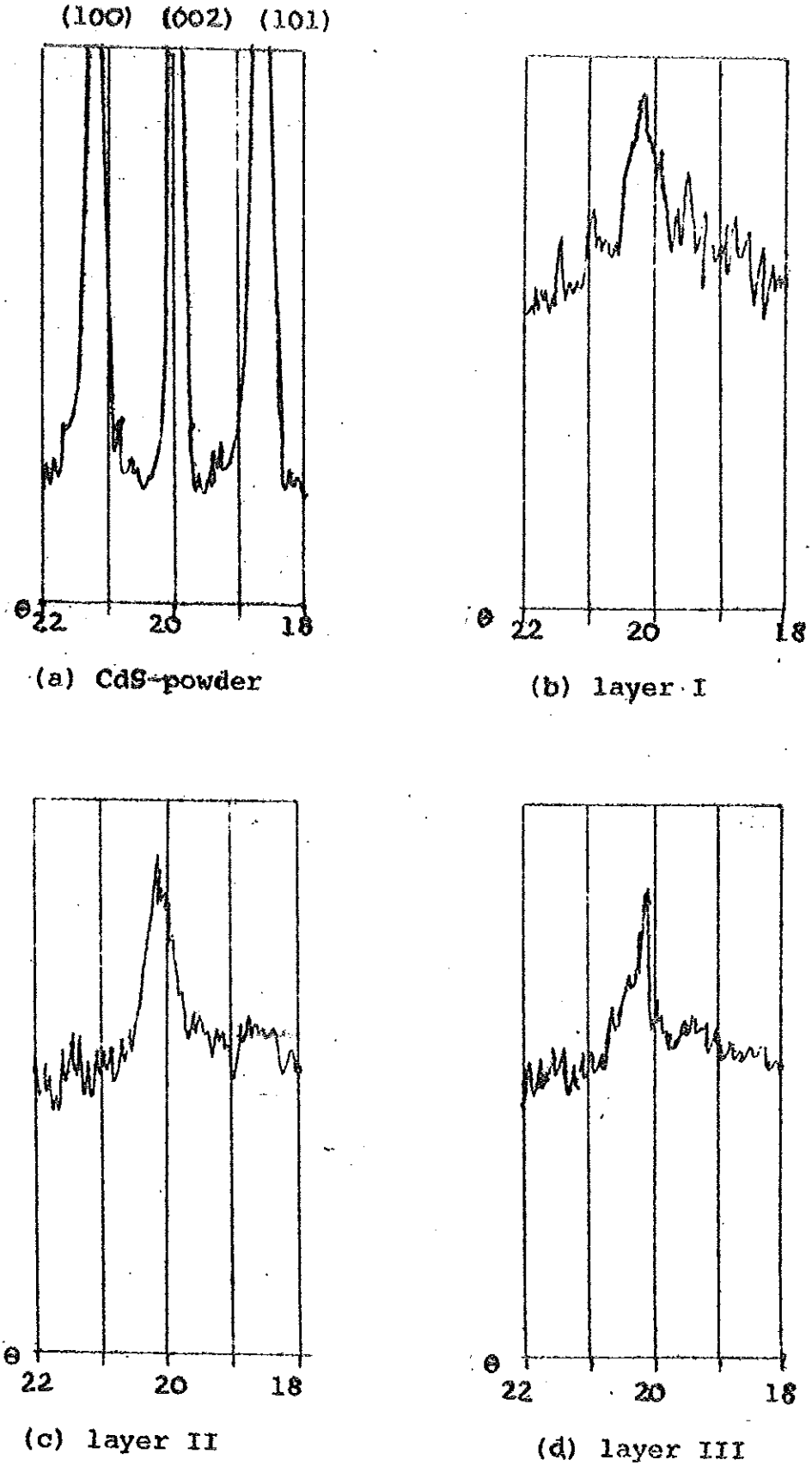

(a) CdS-powder

(b) layer I

(c) layer II

(d) layer III

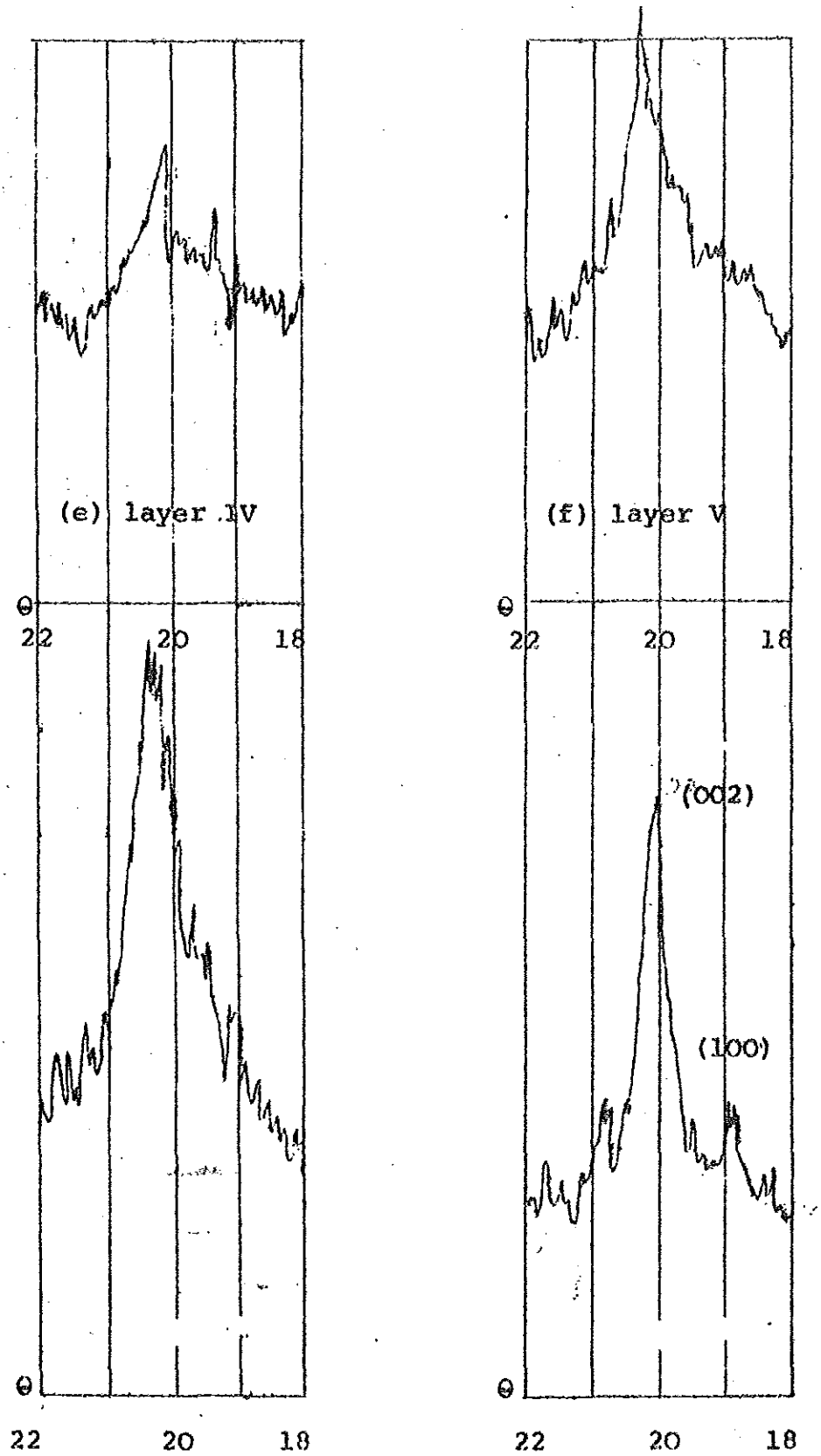
(e) layer IV
(f) layer V
θ
22
20
18
(002)
(100)
(g) layer VI
(h) layer III*

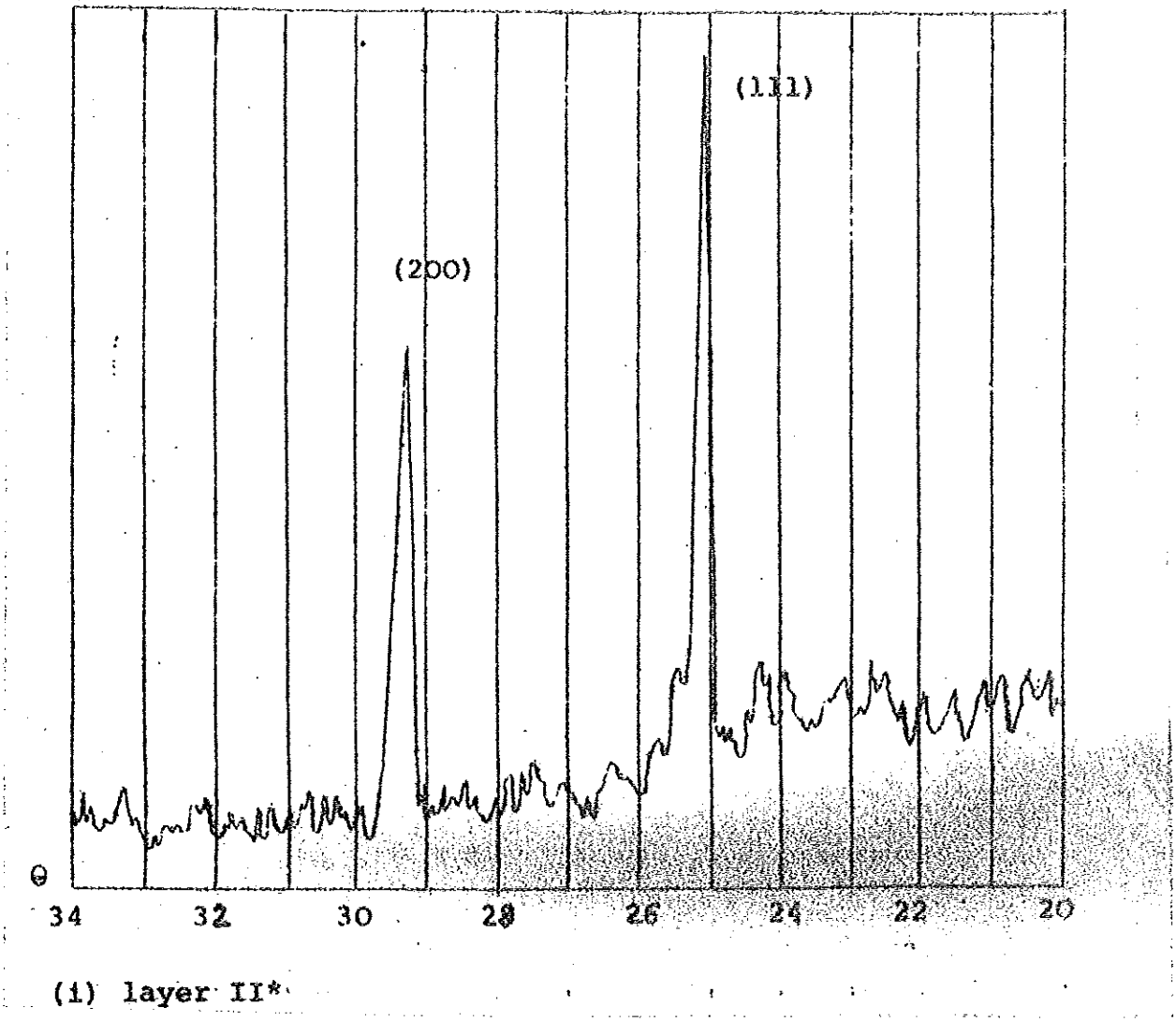

(i) layer II*

The diffraction spectra of all the layers with or without anealing at 120°C are not very sharp, similar to those of amorphous semiconductors. The lavers can be considered as polycrystalline layers of very small grain dimension. All the layers show a peak at $\theta = 20.25^{\circ}$ (d = 3.31Å) which is more pronounced for the layer VI (Fig. 11(g)).

An anealing at 300°C for 20 min at 0.013 Pa (Fig. 11(i)) enhanced the peak but shifted it to 20.1°(d=3.34Å). This indicates a recrystallization and formation of a hexagonal texture with (002) orientation. An anealing at 550°C in air gave peaks (Fig. 11(h)) at 25.1° and 29.25° in place of the 1st peak at 20.25°. This can be identified as (200) and (111) lines of CdO. Hence, in air, an oxidation of CdS films is unavoidable. The shift of the (002) reflection towards smaller angles due to an increased lattice spacing d(from 3.31 to 3.34Å) after anealing can be explained as follows: The preparation of the films from an aqueous dispersion leads to an inclusion of H_2O molecules into the layer in quite a large amount, which are responsible for the formation of nearly amorphous structure for they interrupt the growth of large crystallites. The annealing aimed on a recrystallization and formation of larger crystallites breaks these bindings and replaces them by those of CdS. As a result of annealing H_2O is removed and a structure of a somewhat larger interatomic distance is formed.

One can conclude that the peaks of the layers I - VI (Fig. 11 (b-g)) at 20.25° (d = 3.31Å) correspond to the peak of CdS-powder at 20.0° (3.36Å) which are due to the (002) planes of hexagonal CdS.

CHAPTER 4

ELECTRICAL AND PHOTOELECTRICAL MEASUREMENTS.

4.1 Conductivity Measurements. Contacting.

Conductivity measurements were done using the current-voltage (i-V) method [26] which is based on the measurement of current i flowing through the probe when a voltage V is applied to it by means of electrical contacts. The conductivity σ and the photoconductivity σ_{ph} are derived from Ohm's law, ie.

$$\sigma = \frac{1}{R}\,\frac{\ell}{A} = \frac{\ell}{VA} \cdot i \qquad (55)$$

$$\sigma_{ph} = \Delta\sigma = \frac{\ell}{VA} \cdot \Delta i_{ph} \qquad (56)$$

where R, ℓ and A represent the resistance, the electrode separation and the cross-sectional area of the specimen respecively. The geometrical dimensions ℓ and A can be obtained using a microscope as described in part 3.3.

In performing the measurements a coplanar geometry of the contacts was used. The contacts should not introduce an additional resistance so that the i-V characteristics displays the resistivity of the specimen. Such contacts are called ohmic contacts in contrast to rectifying contacts which arise due to the presence of an electrostatic barrier (space-charge-region) between the metal and the semiconductor [1,27].

In order to attain an ohmic contact with n-CdS, Bube [1] imposes two conditions:

a) A metal with a work function (ϕ_m) smaller than that of n-CdS (ϕ_s) should be chosen.

b) The metal used should act as a donor impurity. Some diffusion of the metal into the semiconductor improves the quality of the contact.

It is shown in Fig. 12 how the condition $\phi_m < \phi_s$ leads to an ohmic contact for an n-type semiconductor.

Possible materials that can be used to make an ohmic contact with CdS are gallium, indium, silver, indium-tin-oxide (ITO) and tin oxide [1,18,28]. Here soldered indium contacts and contacts made from silver paste were utilized.

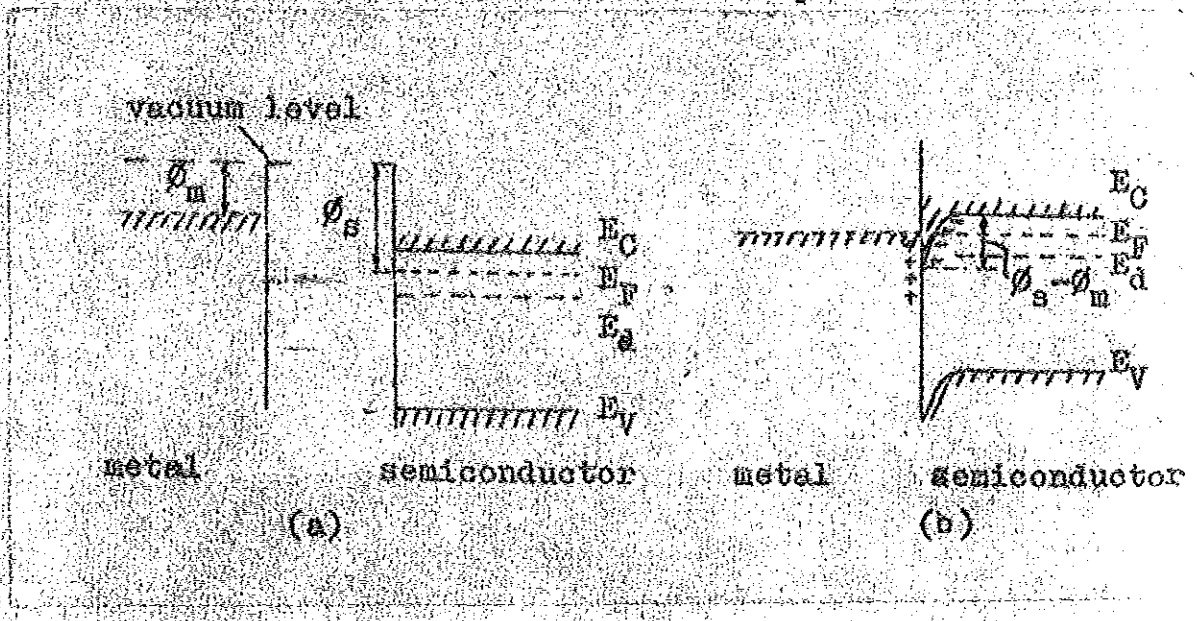

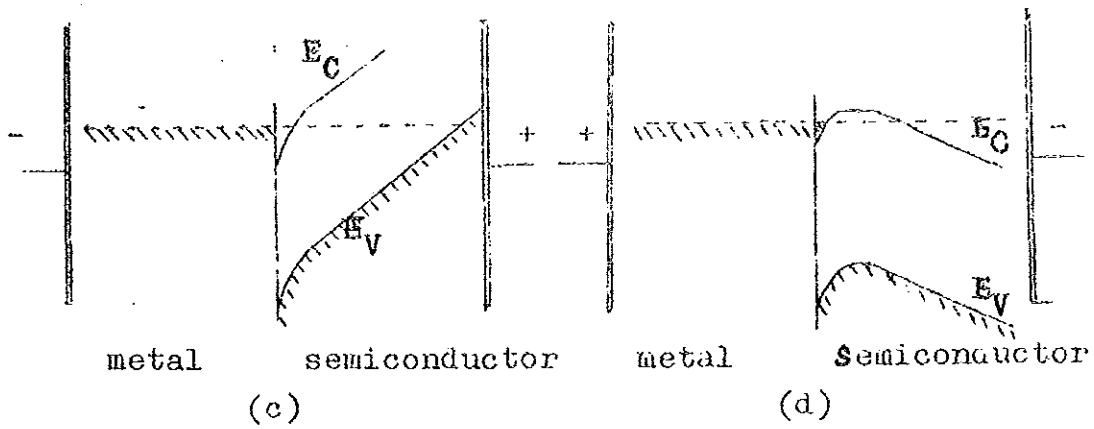

Fig. 12: Energy level diagrams and ohmic metal-n-type semiconductor contact with $\phi_m < \phi_s$ [6]

a) before contact (b) after contact

c) when metal is negatively biased

d) when metal is positively biased.

4.2 Light Sources.

The magnitude of the photoelectric effect depends not only on the total energy of the incident photon flux but also strongly on its spectral energy distribution. Therefore, information about the spectral characteristics of the light sources utilized for photoconductivity measurements have to be supplemented.

Measurements of photoconductivity are done either under the so-called "white light" illumination, (which is realized mostly by an incandescent tungsten filament lamp) or under monochromatic illumination. In the first case, a normalization with respect to a constant energy flux as well as a

constant number of incident photons is common. Both an incandescent tungsten filament radiation (220V, 150W, 2100&m) and monochromatic light (incandescent tungsten radiation plus grating monochromator) were utilized.

The spectral energy distribution of an incandescent lamp can be expressed by means of its spectral emissivity $e(\lambda, t)$, which is the ratio of the spectral emittance of the radiator $M(\lambda, T)_{tung}$ to that of a black-body radiator at the same temperature $M(\lambda, T)_{black}$. For tungsten $e(\lambda,T)$ is given by G. Wyszecki and W.S. Stiles [29]. The curves

$$M(\lambda,T)_{tung} = e(\lambda,T)M(\lambda,T)_{black} \qquad (57)$$

are plotted for different temperatures in Fig. 13.

All spectral photoconductivities were normalized to a constant number of 10^{13} photons incident per second and mm^2.

The spectral energy distribution of the 150W tungsten bulb was measured by means of two different metal interference filters (504 and 644 nm) of known transmittance combined with an infrared absorbing filter and a vaccum thermopile VTh8 (Carl Zeiss Jena, reciever area 7.1 mm^2, sensitivity 4.6V/W). Comparison of the relative intensities found at the different wavelengths with the curves of Fig. 13 gave an approximate filament temperature of 2400K. The total intensity in a distance of 15 cm amounts to 156 mW/cm^2.

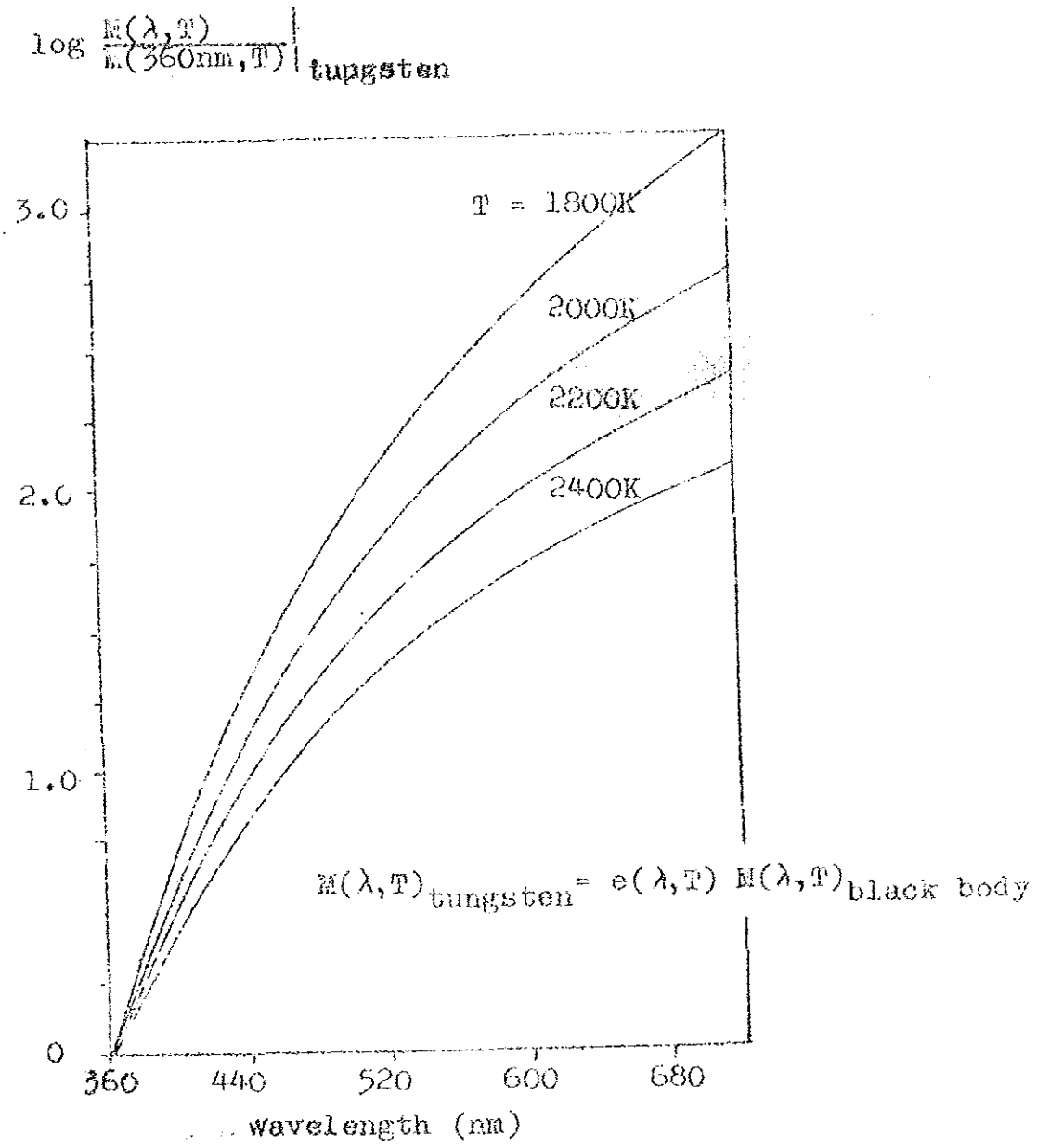

Fig. 13: Relative spectral energy distribution of incandescent tungsten lamp.

The spectral energy distribution of the monochromator (operating voltage of the tungsten lamp 5,6V) emerging from the exit slit of the grating monochromator was also determined with the same thermopile VTh8. The results are represented in Fig. 14 in number of incident photons per time

and area. Obtained spectral photoconductivities were normalized by these values.

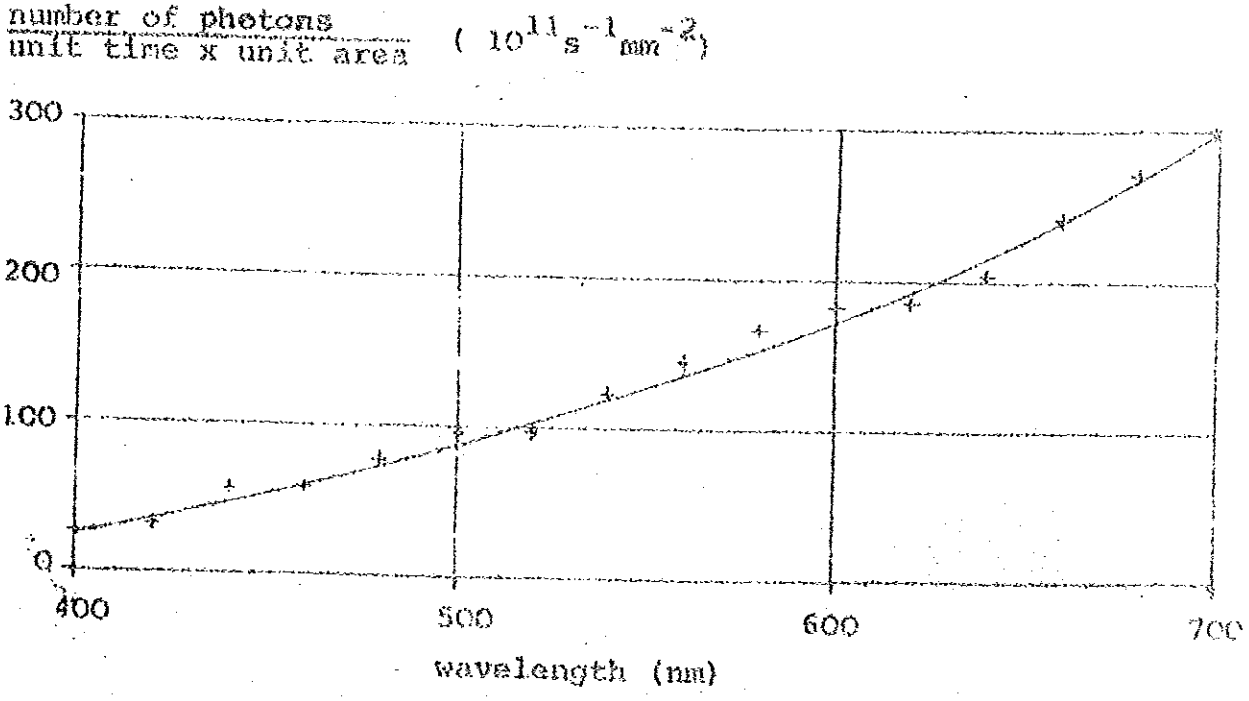

Fig. 14: Spectral distribution of the number of incident photons per time and area of the monochromator.

4.3 Design and Application of a Measuring Amplifier.

The dark resistance of several samples turned out to be so high that the resulting small currents could not be measured accurately by the galvanometers available. This made necessary the application of a measuring amplifier which has to be designed, assembled and tested. A voltage amplifier was proposed that utilizes the potential drop across a 10kΩ series resistor R due to these small currents. To realize an input resistance (R_{in}) much larger than 100kΩ, a MOSFET with an input resistance greater than 10^{12}Ω was included (see Fig. 15).

The MOSFET feeds an operational amplifier of amplification factor (A) adjusted by the external components R_1 and R_2 ($A = \frac{R_1}{R_2}$).

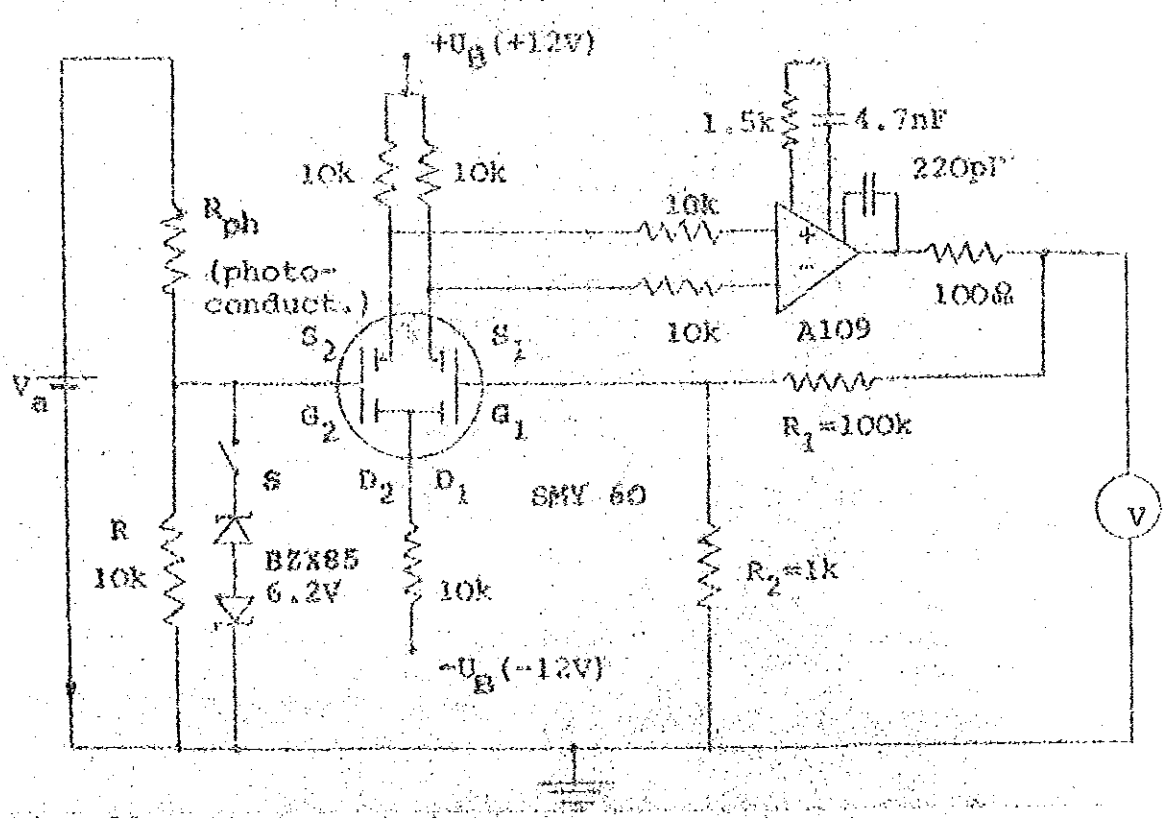

Fig. 15: Circuit of the measuring amplifier

A switch (S) was included to prevent the application of excess voltage by opening it during the measurements.

The output voltage V_{out} of the operational amplifier measured with a digital multimeter amounts to

$$V_{out} = A \cdot V_{in}$$

where V_{in} is the potential drop across the resistor R, which with a known applied voltage V_a gives the resistnace of the photoconductor,

$$R_{ph} = R\left(A \frac{V_a}{V_{out}} - 1\right) . \qquad (58)$$

Because of the tolerance of the resistors R_1 and R_2 the linearity of the amplification factor (A) of the amplifier was determined experimentally by applying a known voltage V_{in}. The resulting output voltages are shown in Fig. 16. The operational amplifier possesses an offset voltage of 940mV, which is to be subtracted from the output reading. It operates linearly for output voltages $|V_{out}| < 5$ V with an amplification factor of 96.5.

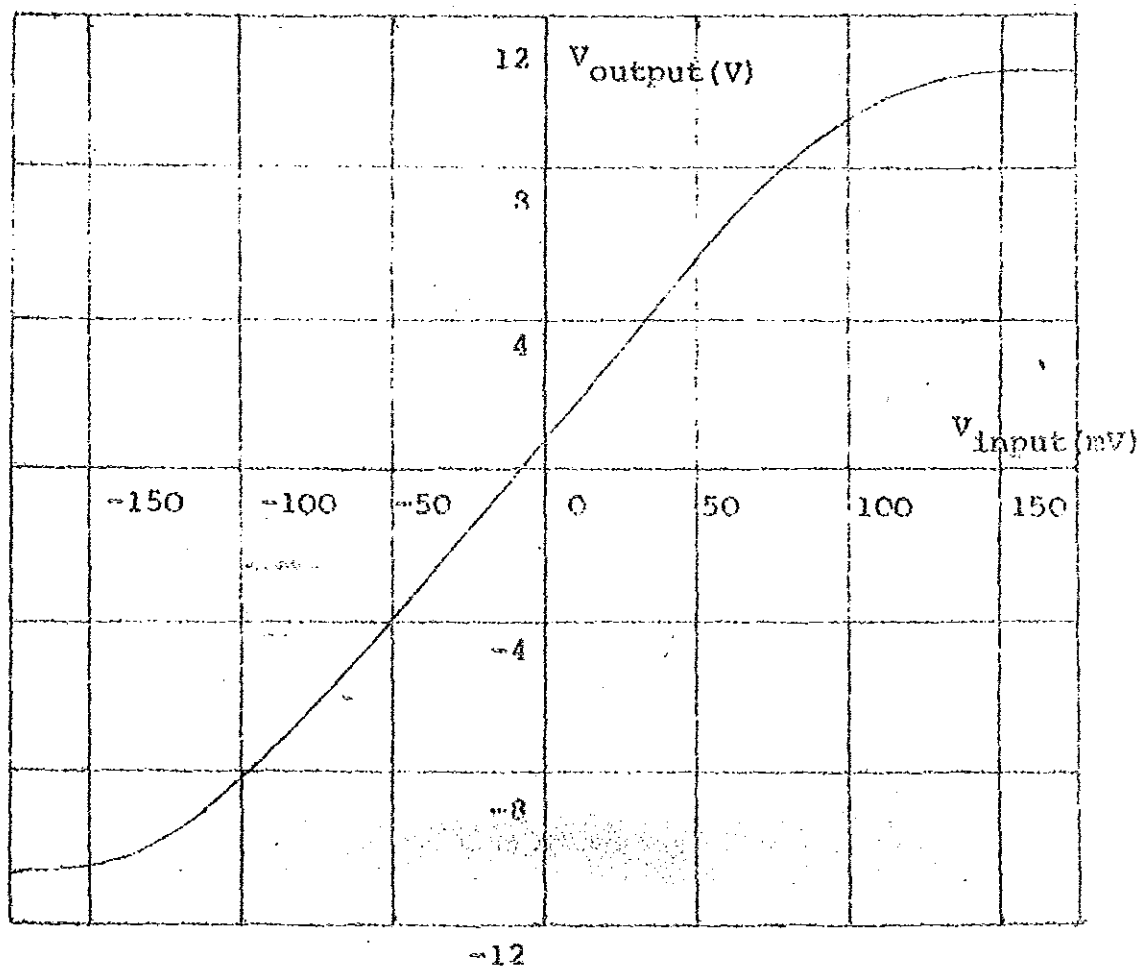

Fig. 16: Measured V_{out}/V_{in} relationship of the operational amplifier.

4.4 Results of Measurement

4.4.1 Light-dark Conductivity Ratio of White Light Illumination.

Together with the layers prepared by chemical deposition technique, monocrystalline CdS photoconductor (VEB Carl Zeis Jena), polycrystalline sintered CdS photoconductor (type WK 65036) and pressed CdS powder were investigated.

Besides the spectral sensitivity, the ratio between the light and dark conductivity is an important property of a photoconductor. The values obtained under white light illumination are the following:

	$\sigma_{light}/\sigma_{dark}$
Monocrystalline CdS	113
Polycrystalline WK 65036	10^6
Layer 6a (OC)	20
Layer 6b (OC + annealed)	11
Layer 16 (OC + Li doped)	12
Layer 17 (OC, Li doped, double bath)	1,4
Pressed CdS	16
Pressed CdS (annealed)	1,2
Pressed CdS (NaCl doped, annealed)	2,6

In order to attain a large light/dark conductivity ratio, the dark conductivity should be as small as possible. This can be reached if there are no impurities (intrinsic behaviour) or if the donor impurities are compensated.

The first type is realized in the monocrystalline CdS photoconductor for which only interband transitions are possible (excitation 1, Fig. 1) which is confirmed by the spectral measurements. Doping reduces the ratio as can be noted by comparing the values of the layer 16 with that of the undoped layer 6a. In the case of annealing, the dark conductivity increases more faster than the photoconductivity thus resulting in a decrease of the ratio of the light to dark conductivity which is indicated by comparing 6a and 6b, and by annealing pressed CdS. The high value for the photoconductor WK 65036 is probably due to a very high doping concentration of both donors and acceptors so that a tremendous number of states exist inside the bandgap. In the dark the photoconductor is compensated and the dark conductivity is small. Under illumination transitions of the type 2 and 3 (Fig. 1) are possible thus resulting in an increase of the photoconductivity.

4.4.2 Spectral Photoconductivity.

In Fig. 17 (a-j) the spectral photoconductivity responses of the samples investigated are shown. For monocrystalline CdS (Fig. 17 (a)) an edge is indicated at 517 nm which implies the photoconductor's sensitivity for wavelengths greater than 520 nm is low. Since only interband transitions are indicated, the CdS crystal is of high purity.

The spectral response of the polycrystalline CdS (WK 65036) photoconductor (Fig. 17 (b)) showed a strong sensitivity at wavelengths greater than 550 nm which corresponds to smaller photon energies. This photoconductor does not indicate a bandgap at 2.4 eV as monocrystalline one. This can be explained by nothing but the transitions that take place within the band-gap due to lots of impurities (which have been mentioned earlier) and for that reason the sensitivity of the WK 65036 is high in that spectral region.

Pressed CdS powder, annealed, doped, doped and annealed samples have been investigated. The dark - conductivity of first sample is high and doping shifts the maximum from 625 to 575 nm. Annealing of the undoped and doped samples increases the respective sensitivities for longer wavelengths. This indicates that states inside the band-gap are activated for absorption/generation processes.

For the crystalline CdS, polycrystalline WK 65036 CdS and the pressed CdS powder, the conductivity measurements were only in relative units, for the active thickness of the samples cannot be determined. On the other hand, photoconductivity of the films 4a, 6b, 16 and 17 (Table 1) have been calculated in absolute units. Fig. 17 (c) gives the spectral photoconductive response of the layer 4a. Annealing (17 (d)) leads to two possible results. At first the photoconductive sensitivity increases by about one order and

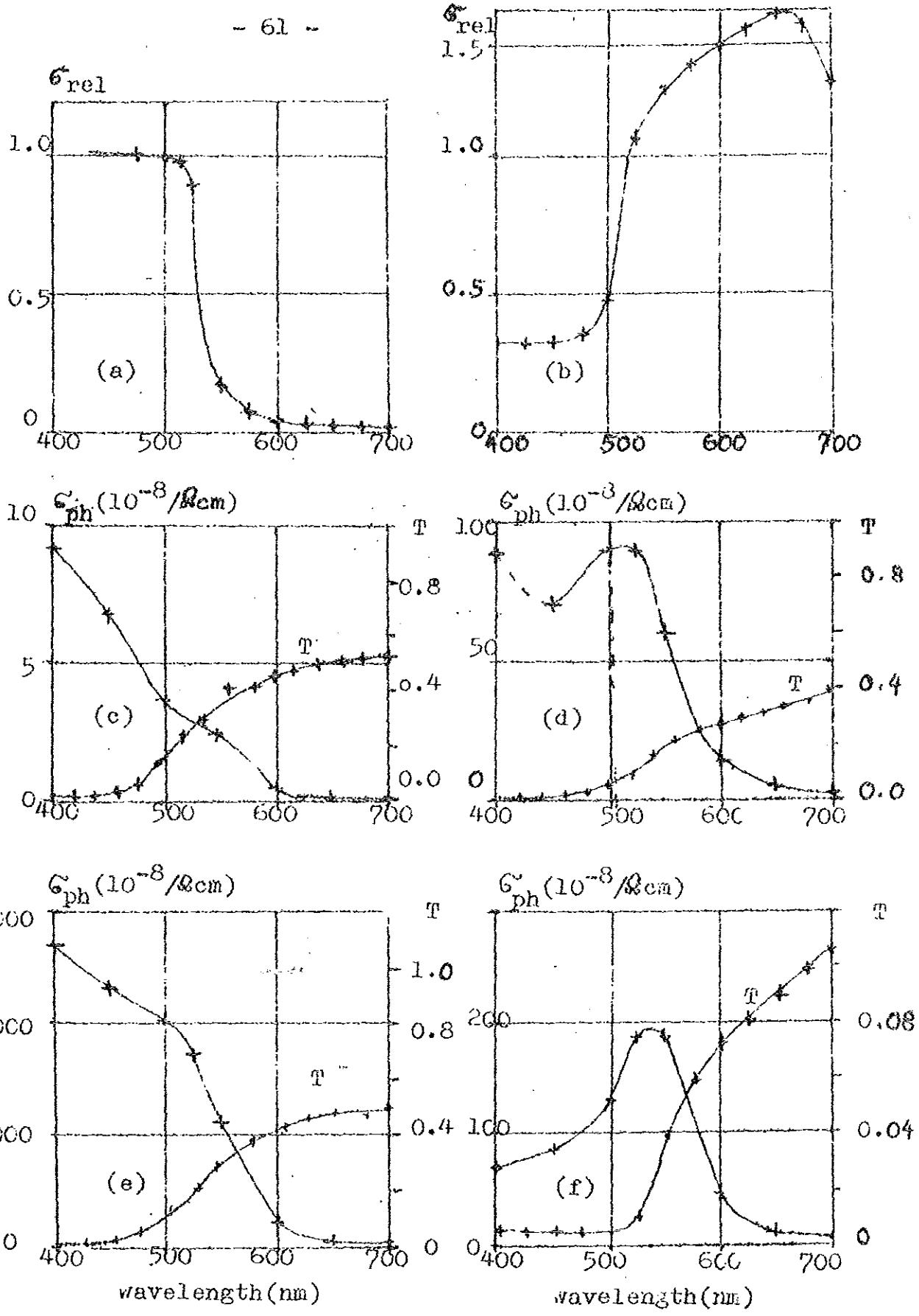
σrel
1.0
0.5
0
(a)
400
500
600
700
σrel
1.5
1.0
0.5
0
(b)
400
500
600
700
σph(10⁻⁸/Ωcm)
10
5
0
T
0.8
0.4
0.0
(c)
400
500
600
700
σph(10⁻⁸/Ωcm)
100
50
0
T
0.8
0.4
0.0
(d)
400
500
600
700
σph(10⁻⁸/Ωcm)
3000
2000
1000
0
T
1.0
0.8
0.4
0
(e)
400
500
600
700
wavelength(nm)
σph(10⁻⁸/Ωcm)
200
100
0
T
0.08
0.04
0
(f)
400
500
600
700
wavelength(nm)

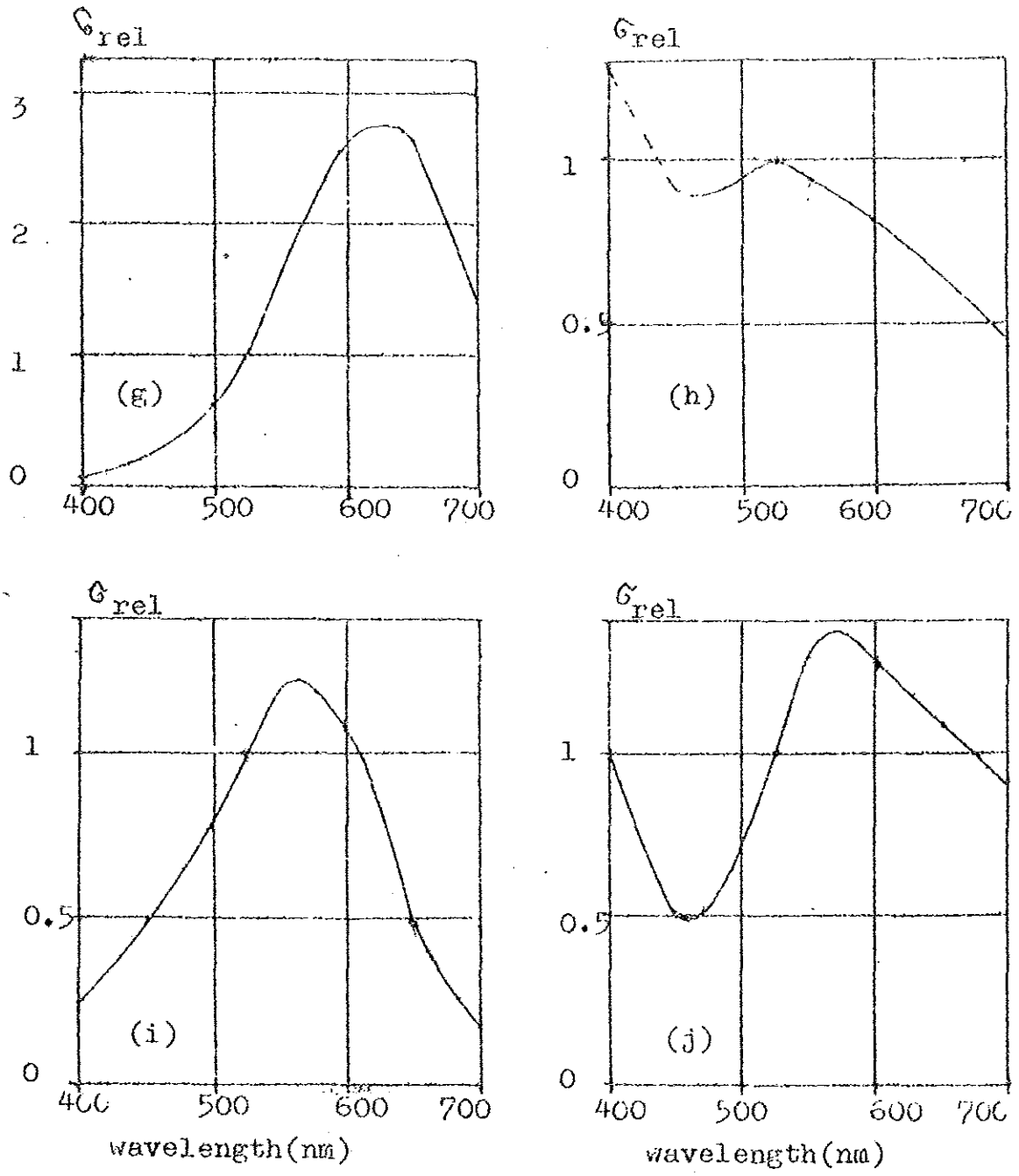

Fig.17: Spectral Photoconductivity of
(a) monocrystalline CdS, (b) polycrystalline CdS (WK 650)
(c) layer 4a, (d) layer 6b, (e) layer 16,
(f) layer 17, (g) pressed CdS, (h) pressed and annealed Cd
(i) pressed CdS, doped with NaCl, (j) the same as (i) but also annealed.
T: spectral transmittance curve

secondly a distinct edge at about 2.4 eV appears. Both can be explained by the formation of larger crystallites as a result of annealing in agreement with the X-ray structure investigations (part 3.4).

The photconductive response of the doped layers 16, and 17 are shown in Fig. 17 (e-f), from which one can see that the overall sensitivity is larger than that of the unannealed film 1a, one can realize from Fig. 17 (f) that double bath deposition does not give layers of simply increased thickness, but the physical properties of the additionally deposited part is different from those of a single deposition. This was noticed in making the contacts because weak tensions were sufficient to disattach the contacts. Probably, the upper part of the layer contains microvoids in addition to crystal imperfections that reduce the mechanical strength. The electrical properties are also influenced by these microvoids, for the resistance increases which could be due to the reduction of the available cross-section for current conduction. Since almost all of the light absorption occurs in these region, generation of free charge carriers takes place in this part, and the mobility of these carriers will be reduced due to these microvoids.

The spectral transmittance $T(\lambda)$ of the investigated layers is also shown in Fig. 17 (c-f). The presence of an absorption edge is reflected by the increase or decrease of the transmittance at those values where absorption occurs.

The spectral transmittance $T(\lambda)$ and the photoconductive response σ_{ph} curves have been used to calculate the spectral variation of the absorption efficiency $\eta(\lambda)$ (eq. 49) of the layer 6b. The absorbance $A(\lambda)$ of the film has to be known in order to be able to calculate η. Since the transmittance and absorbance (eq. 47) depend on the optical constants N and K, it is impossible to evaluate both N and K from the single quantity. The values of N for CdS given by K.W. Boer [30] were used.

Using the same reasoning in approximating the absorbance A(eq. (47)), the transmittance T can be written as

$$T = (1-R_1)(1-R_2)(1-R_3)e^{-\alpha d}. \qquad (59)$$

This can be used to calculate the absorption index K (and the absorption coefficient ($\alpha = \frac{4\pi K}{\lambda}$), which are contained in R_1 and R_2. The results are presented in Fig. 18 (a). Knowing $N(\lambda)$ and $K(\lambda)$ the approximated reflectance R can be determined.

The absorbance as given by eq. 37 can be rewritten in the form

$$A(\lambda) = 1 - \{T(\lambda) + R(\lambda)\}.$$

The reflectance R, the absorbance A and transmittance T of the layer 6b are given in Fig. 18 (b).

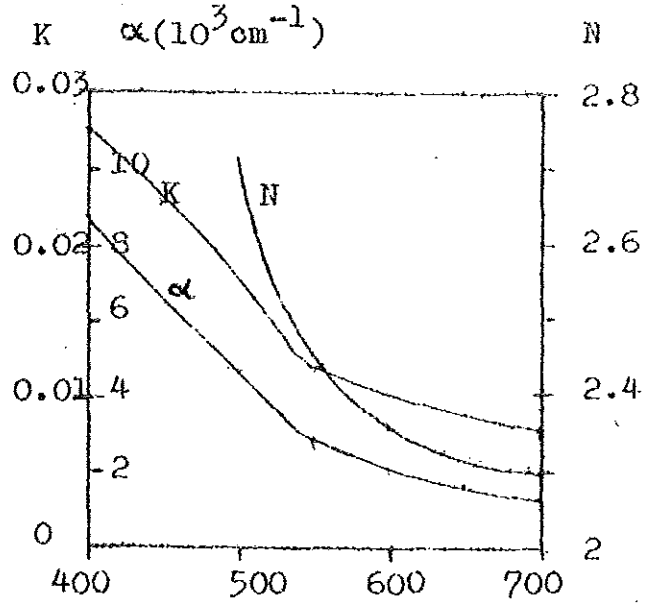

(a)

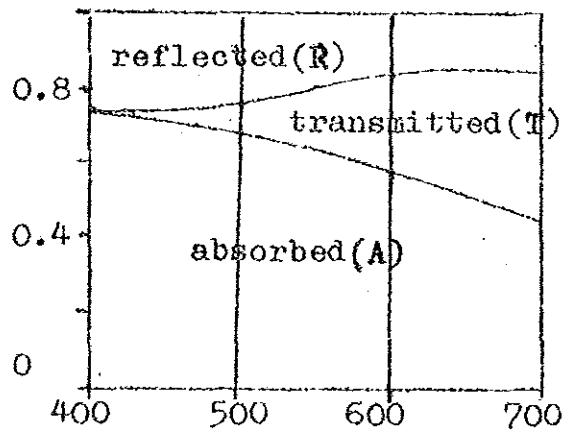

(b)

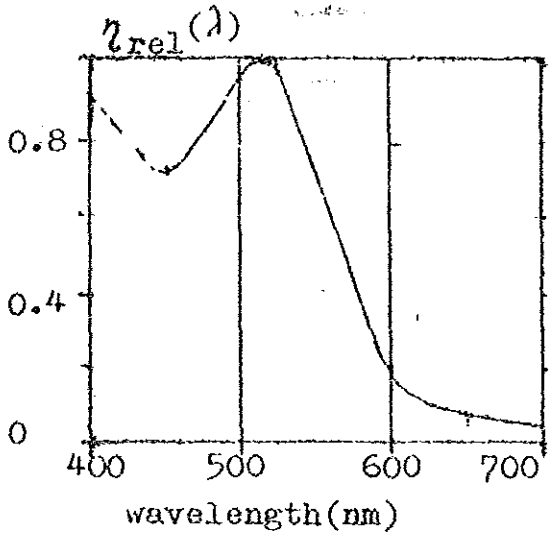

(c)

Fig.13:
(a) Optical constants of layer 6b,
(b) spectral reflectance, transmittance and absorbance,
(c) relative quantum-efficiency

The quantity $(\frac{I_o}{h\nu})$ in eq. (49) is constant due to the normalization of the spectral photoconductivity and thus one can write

$$g = \eta \cdot \text{const} \cdot \frac{A}{d}$$

Assuming that the photoconductivity is due to carrier concentration (Δn)

$$\Delta\sigma = \sigma_{ph} = e\mu_n \Delta n$$

where Δn stands for the saturation value (eq. 18),

$$\Delta n = g\tau$$

The quantum efficiency η_{rel} is then

$$\eta_{rel} = \frac{\sigma_{ph}(\lambda)}{A(\lambda)} \Big/ \frac{\sigma_{ph}(\lambda_{ref})}{A(\lambda_{ref})} \qquad (61)$$

The curve of $\eta_{rel}(\lambda)$ is presented in Fig. 18 (c) for $\lambda_{ref} = 517$ nm.

η_{rel} exhibits an edge, and inspite of relatively high absorption for longer wavelengths {Fig.18 (c)}, the resulting photoconductivity is small because η_{rel} drops strongly.

4.4.3 Life Time Determination by Photoconductive Decay.

The carrier life time was determined by photoconductive decay, ie. decay of the photocurrent after switching off the illumination. For short life times, intermittent white-light radiation was produced by a light chopper while for longer life times, the decay was plotted by a chart-speed-recorder. The decay curves $\sigma_{ph}(t)/\sigma_{ph}(0)$ of the monocrystalline CdS and polycrystalline WK 65036 photoconductors are given in Fig. 19.

The related life times as calculated from eq. (19) are the following:

Monocrystalline CdS	2,5	ms
Polycrystalline CdS WK 65036	6	ms
Pressed CdS	3	ms
Layer 6b	5	s
Layer 16	54	s

The monocrystalline and the pressed CdS yield small life times while films prepared by chemical bath deposition method exhibit very large lifetimes. The lifetimes have a spectral dependence which is clearly indicated by layer 16.

The lifetime increases than its value at the bandgap energy for both an increase or a decrease in wavelength.

Fig.19: Examples of the decay of photoconductivity
(a) monocrystalline CdS
(b) polycrystalline CdS (#K65036)
(light switched off at t=0s)

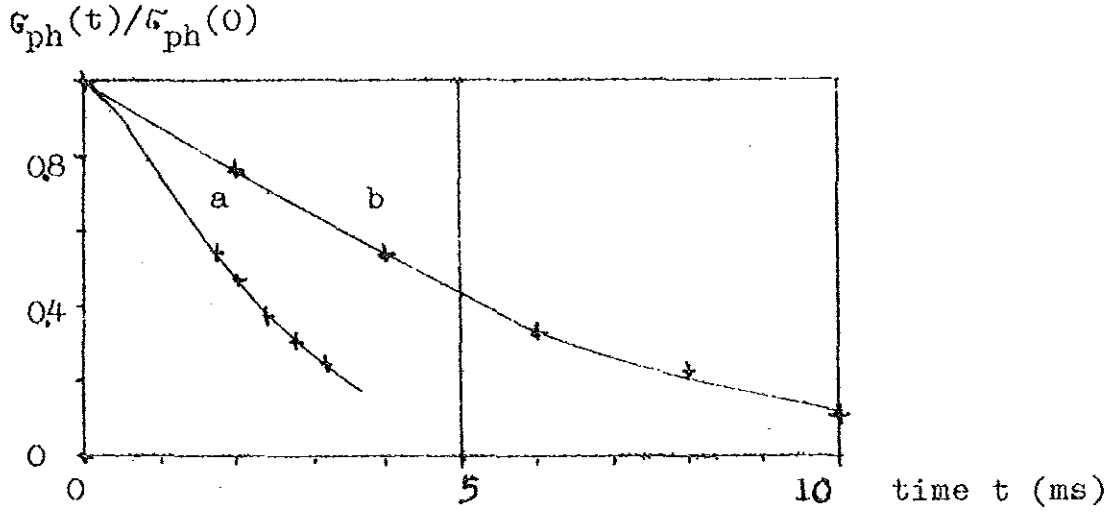

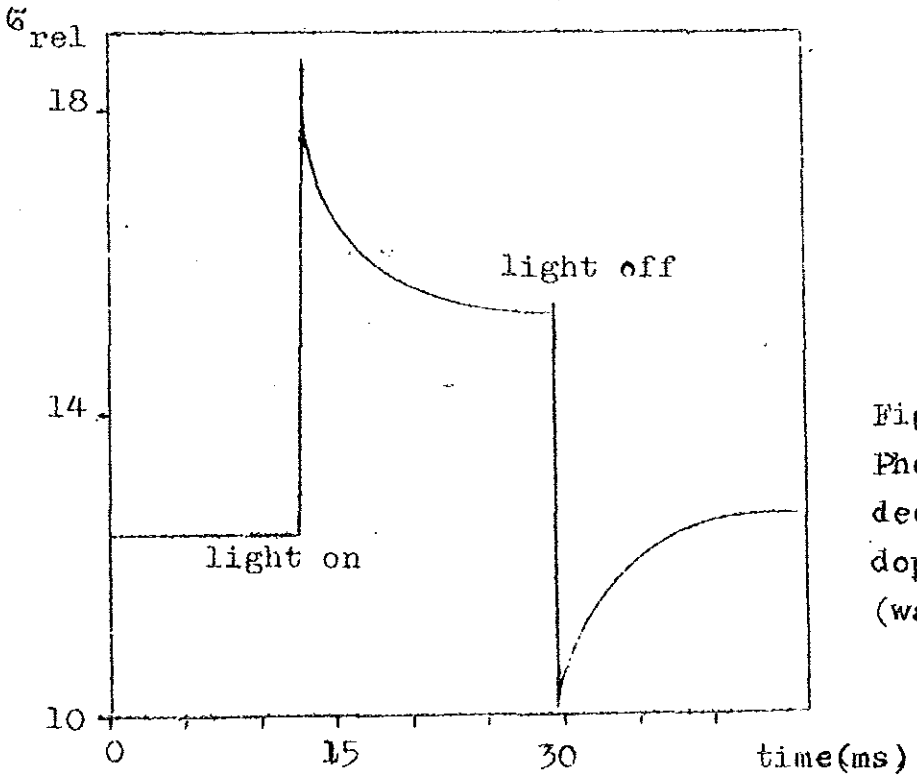

Fig.20:
Photoconductive decay of pressed CdS doped with NaCl
(wavelength: 600nm)

Wavelength (nm)	Time (sec)
400	75
450	45
500	33
550	34
600	49
650	87
700	170

A different decay behavior was observed when pressed CdS doped with NaCl was illuminated with light of wavelength 600 nm. There appeared a sharp edge which then decreases to a saturation value. This is followed by a sudden decrease at switch off which again exhibits a sharp increase to another saturation value (see Fig. 20).

It was not possible to measure the mobility and its changes under illumination for the resistance of the prepared CdS layers was large ($\approx 10^8 \Omega$).

CONCLUSION

In this dissertation the photoconductivity of cadmium sulfide has been discussed theoretically and investigated experimentally. A photoconductive response is observed both in monocrystalline one and polycrystalline cadmium sulfide, though its magnitude is reduced for the polycrystalline CdS. This can be explained by the grain boundary trapping which can influence both the carrier mobility and carrier concentration. According to theory of conductivity and photoconductivity in polycrystalline materials, the average number of free charge carriers is very small if the trap concentration per area (Q_t/L_g) is larger than the doping concentration N_d. Eventhough it is not in the procedure to find the trap and doping concentrations quantitatively , yet it is possible to say that the trap concentration (Q_t/L_g) is much larger than the doping concentration. This is as well supplemented by the low conductivity values obtained which forced us to use an operational amplifier with a very high input resistance.

The structure of the layers from X-ray diffraction is hexagonal of very small crystallites (with very small grain dimension) very close to the amorphous structure. The smaller the crystallite size the greater the number of crystallites of a layer of certain thickness and the greater the number of grain boundaries. This decreases the dark and photoconductivity thus increasing the resistance of the sample under consideration.

The monocrystalline CdS photoconductor exhibits a decrease in photoconductivity beyond the bandgap. But the WK 65036 polycrystalline CdS and the prepared ones show a photoconductive response for longer wavelengths. This can be explained by the fact that for monocrystalline CdS interband transitions are dominant while for the polycrystalline ones a large number of states occur in the bandgap which are responsible for the photoconductive response at longer wavelength (or smaller energies).

The curves of the photoconductive response, the transmitance, absorbance and absorption coefficient curves of polycrystalline CdS are in complete agreement with each other defining either a sudden fall or a sharp increase at the bandgap energy.

The light-dark conductivity ratio of the prepared layers is about 10. It is more for the undoped than that of the doped polycrystalline layer.

References

1 R.H. Bube, Photoconductivity of Solids, John Wiley and Sons Inc. New York, 1960

2 Proceedings International Conference on Semiconductor Physics Prague, 1960, Czechoslovak Academy of Sciences, Prague, 1961.

3 S. Martinuzzi, Solar Cells, 5 (1982) 243.

4 R. H. Bube, F. Buche, A.L. Fahren Buch, Y.Y.Ma, K.W. Mitchell, IEEE Transactions on Electron Devices ED 24 (1977) 487

5 P.S. Kireev, Semiconductor Physics, Mir Publishers Moscow, 1960

6 L.V. Azaroff, Introduction to Solids, MCGAW-Hill Book Company INC. New York, 1960

7 C. Kittel, Introduction to Solid State Physics, John Wiley and Sons, New York, (1976)

8 T.J. Couts, Active and Passive Thin-film devices, Academic Press London, 1978

9 H.E. Backus, Solar Cells, IEEE Press New York, 1976

10 K.L. Petritz, Phys. Rev. 104 (1956) 1508

11 S. Esperik, C.H. Wu, R.H.Bube, J. Appl. Phys. 42 (1971) 3513

12 J.Y.W.Seto, J. Appl. Phys. 46 (1975) 5247

13 J. Volger, Phys. Rev. 110 (1950) 1023

14 J.W. Orton B.J. Goldsmith, J.A. Chapman, M.J. Powell., J. Appl. Phys. 53 (1982) 1602

15 H.C. Card, Solid State Electronics 25 (1982) 505

16 M.Born and E. Wolf, Principles of Optics, pergamon Press, New York, 1970

17 W. Petrowa, K.H. Stoetzel, W. Tuebner, G. Kluge, P. Sueptitz, Phys. Stat Solidi (A), 62 (1980) 249

18 M. Savellš, J. Bougnot, H. Lunguet, M. Perotin, O. Maris, C. Gril, Solar Cells 5 (1982) 213

19 M. Matsmoto, N. Nakayama, S.Ikeyami, J. Appl. Phys 19 (1980) 129

20 G.A. Kitaw, S.G. Mokrushin, A.A. Vritskaya, Colloid J. USSR 27 (1965) 38

21 A.G. Shikalzar, S.H. Pawar, Solid Commun. 32(1979)361

22 W.R.Coak L. Shiozawa E. Augustine, J.Appl.Phys. 41 (1970) 3058

23 H.E. Swanson, R.K. Fuyat, G.M. Ugrinic, Standard X-ray diffraction powder patterns, NBS Circular, Vol.IV, 1955

24 Peter Gray, Crystalline State, Oliver and Boyd Edinburg, 1972

25 H.E. Swanson, R.K. Fuyat, Standard X-ray Diffraction Powder Patterns, NBS Circular 539, Vol.II 1953

26 K. Lark-Horovitz and V.A. Johnson, Methods of Experimental Physics, Solid State Physics, Academic Press New York, 1959.

27 E.H. Rhoderick, IEEE Proc 219 (1982) 1

28 R.O. Loufty, L.M. McIntyre, D.K. Musti C.K. Hsiao, Solar Energy Materials 5 (1981) 221

29 G. Wyszecki, W.S. Stiles, Color Science, John Wiley and Sons INC. New York 1967

30 K.W. Boer, Conference of the Am. Section of the Int. Solar Energy Society, Winnepeg 1976 p.130.

DECLARATION

I, the undersigned, declare that this thesis is my work and that all sources of materal used for the thesis have been duly acknowledged.

Name_____

Signature_____

Date of Submission_____